Cell Metabolism

Article

A macrophage-hepatocyte glucocorticoid receptor axis coordinates fasting ketogenesis

Graphical abstract

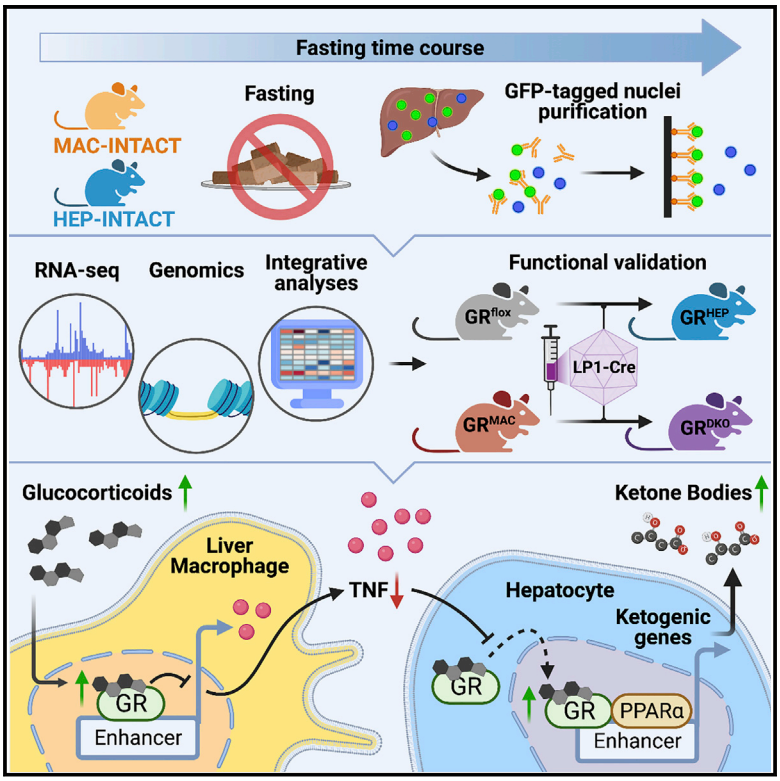

Highlights

- Mutual intercellular crosstalk shapes the hepatic transcriptional response to fasting
- Macrophage GR regulates ketogenesis during fasting and endotoxemia
- Macrophage GR promotes cooperative GR/PPARα target gene activation in hepatocytes
- Macrophage GR suppresses TNF and facilitates nuclear translocation of hepatocyte GR

Authors

Anne Loft, Søren Fisker Schmidt, Giorgio Caratti, ..., Anja Zeigerer, Jan Tuckermann, Stephan Herzig

Correspondence

sfs@bmb.sdu.dk (S.F.S.), jan.tuckermann@uni-ulm.de (J.T.), stephan.herzig@helmholtz-muenchen.de (S.H.)

In brief

Fasting metabolism and immunity are tightly linked; however, little is known about how immune cells engage in fasting homeostasis in healthy subjects. Using a cell-type-resolved genomics approach, Loft et al. demonstrate how glucocorticoid signaling in resident liver macrophages directly influences glucocorticoid signaling and ketogenesis in hepatocytes during fasting.

Loft et al., 2022, Cell Metabolism *34*, 473–486
March 1, 2022
https://doi.org/10.1016/j.cmet.2022.01.004

CellPress

Cell Metabolism

CellPress

Article

A macrophage-hepatocyte glucocorticoid receptor axis coordinates fasting ketogenesis

Anne Loft,[1,2,3,4,5,6,14] Søren Fisker Schmidt,[1,2,3,4,5,6,14,*] Giorgio Caratti,[7,14] Ulrich Stifel,[7] Jesper Havelund,[5] Revathi Sekar,[1,2,3,4] Yun Kwon,[1,2,3,4] Alba Sulaj,[4,8] Kan Kau Chow,[1,2,3,4] Ana Jimena Alfaro,[1,2,3,4] Thomas Schwarzmayr,[9] Nikolaj Rittig,[10,11] Mads Svart,[10,11] Foivos-Filippos Tsokanos,[1,2,3,4] Adriano Maida,[1,2,3,4] Andreas Blutke,[12] Annette Feuchtinger,[12] Niels Møller,[10] Matthias Blüher,[13] Peter Nawroth,[2,8] Julia Szendrödi,[2,8] Nils J. Færgeman,[5] Anja Zeigerer,[1,2,3,4] Jan Tuckermann,[7,*] and Stephan Herzig[1,2,3,4,15,*]

[1]Institute for Diabetes and Cancer, Helmholtz Center Munich, Neuherberg 85764, Germany
[2]Joint Heidelberg-IDC Translational Diabetes Program, Internal Medicine, Heidelberg University Hospital, Heidelberg 69120, Germany
[3]Molecular Metabolic Control, Technical University Munich, Munich 80333, Germany
[4]German Center for Diabetes Research, Neuherberg 85764, Germany
[5]Department of Biochemistry and Molecular Biology, University of Southern Denmark (SDU), Odense 5230, Denmark
[6]Center for Functional Genomics and Tissue Plasticity (ATLAS), SDU, Odense 5230, Denmark
[7]Institute for Comparative Molecular Endocrinology, Universität Ulm, Ulm 89081, Germany
[8]Department of Endocrinology and Clinical Chemistry, Heidelberg University Hospital, Heidelberg 69120, Germany
[9]Institute of Human Genetics, Helmholtz Zentrum München, Neuherberg 85764, Germany
[10]Department of Internal Medicine and Endocrinology (Multilateral Environmental Agreement) and Medical Research Laboratory, Aarhus University Hospital, Aarhus C 8000, Denmark
[11]Steno Diabetes Center Aarhus, Aarhus University, Hedeager 3, 2nd Floor, 8200 Aarhus N, Denmark
[12]Research Unit Analytical Pathology, Helmholtz Center Munich, Neuherberg 85764, Germany
[13]Helmholtz Institute for Metabolic, Obesity and Vascular Research (HI-MAG), Helmholtz Zentrum München at the University of Leipzig and University Hospital Leipzig, Leipzig 04103, Germany
[14]These authors contributed equally
[15]Lead contact
*Correspondence: sfs@bmb.sdu.dk (S.F.S.), jan.tuckermann@uni-ulm.de (J.T.), stephan.herzig@helmholtz-muenchen.de (S.H.)
https://doi.org/10.1016/j.cmet.2022.01.004

SUMMARY

Fasting metabolism and immunity are tightly linked; however, it is largely unknown how immune cells contribute to metabolic homeostasis during fasting in healthy subjects. Here, we combined cell-type-resolved genomics and computational approaches to map crosstalk between hepatocytes and liver macrophages during fasting. We identified the glucocorticoid receptor (GR) as a key driver of fasting-induced reprogramming of the macrophage secretome including fasting-suppressed cytokines and showed that lack of macrophage GR impaired induction of ketogenesis during fasting as well as endotoxemia. Mechanistically, macrophage GR suppressed the expression of tumor necrosis factor (TNF) and promoted nuclear translocation of hepatocyte GR to activate a fat oxidation/ketogenesis-related gene program, cooperatively induced by GR and peroxisome proliferator-activated receptor alpha (PPARα) in hepatocytes. Together, our results demonstrate how resident liver macrophages directly influence ketogenesis in hepatocytes, thereby also outlining a strategy by which the immune system can set the metabolic tone during inflammatory disease and infection.

INTRODUCTION

The nutritional status influences immune responses, and cellular metabolism plays an important role in immune cell biology with chronic malnutrition causing immunodeficiencies, as illustrated by common infections being a frequent cause of death in undernutritioned children (Bourke et al., 2016). Conversely, controlled caloric restriction or periodic fasting improves the outcomes of multiple inflammatory and autoimmune diseases via metabolic rewiring of immune cells (Okawa et al., 2020). Moreover, during infections, immune cells acutely trigger sickness behavior and metabolic adaptations that confer tissue tolerance to bacterial infections (Ganeshan et al., 2019; Wang et al., 2016; Weis et al., 2017). For example, anorexia was recently shown to protect against bacterial infection by lowering glucose utilization and increasing circulating ketone levels, thereby limiting reactive oxygen species induced by antibacterial inflammation (Wang et al., 2016). Thus, fasting metabolism impacts on both the immune system and the consequences of its activation; however, little is known about the direct influence of immune cells on key metabolic cell types during fasting in healthy subjects and their contribution to homeostatic metabolic control.

During fasting, the liver plays a central role by activating glycogenolysis/gluconeogenesis- and fatty acid oxidation (FAO)/ketogenesis-related gene programs to generate energy substrates

for the brain, muscle, and other peripheral organs. Accordingly, the transcriptional regulation of these programs in the parenchymal hepatocytes has been intensively studied (Goldstein and Hager, 2015). Key fasting activated transcription factors (TFs) include cAMP-response-element-binding protein (CREB), peroxisome-proliferator-activated receptor alpha (PPARα), and the glucocorticoid receptor (GR/NR3C1) (Herzig et al., 2001; Kersten et al., 1999; Opherk et al., 2004) that operate at fasting-induced enhancers to collectively promote the fasting gene programs (Goldstein et al., 2017). In contrast, molecular insights into the fasting response of immune cells in the liver, such as the liver macrophage population, are limited. Furthermore, whereas liver macrophages have been proposed to play a central role in the disruption of glucose homeostasis in pathophysiological conditions such as the metabolic syndrome and obesity (Huang et al., 2010; Lanthier et al., 2010; Stienstra et al., 2010), it is not known whether these cells contribute to metabolic homeostasis during fasting in healthy subjects.

Here, we generated time-resolved profiles of fasting-induced changes in the chromatin and gene landscapes of liver macrophages and hepatocytes and investigated the crosstalk between these cell types. We identified the macrophage GR as a key driver of the dynamic genomic and transcriptional changes in macrophages, including suppression of cytokine expression, and of fasting-induced ketogenesis through potentiation of synergistically activated GR/PPARα target genes in hepatocytes. Our data thereby identify an intercellular nuclear receptor (NR) communication pathway necessary for full execution of hepatic ketogenesis during fasting.

RESULTS

Cell-type-specific profiling of the hepatic fasting response

To investigate the temporal, cell-type-specific changes in the liver during fasting, we applied the "isolation of nuclei tagged in specific cell types" (INTACT) methodology, allowing Cre-lox-driven cell-type-specific labeling and subsequent affinity purification of nuclei from intact tissues (Deal and Henikoff, 2010; Loft et al., 2021a, 2021b; Mo et al., 2015). Specifically, we used HEP-INTACT mice to allow for a selective pull-down of hepatocyte nuclei and MAC-INTACT mice to target the myeloid nuclei within the liver (Figures S1A–S1F). For simplicity, the GFP+ nuclei from MAC-INTACT mice are henceforth termed macrophage nuclei. Importantly, for both HEP-INTACT and MAC-INTACT mice, we confirmed a strong enrichment of established cell-type-specific markers (e.g., *Alb* in HEP-INTACT mice and *Clec4f* in MAC-INTACT mice), whereas markers of the other cellular lineage were depleted in the GFP+ nuclei (Figures S1G and S1H).

We then subjected female HEP-INTACT and MAC-INTACT mice to a fasting protocol starting at the onset of their active phase (ZT12), and after 3, 8, 16, and 24 h, livers were collected for INTACT followed by RNA- and ATAC-seq analyses (Figure S1I). Ad libitum fed controls were sacrificed at each time point to account for diurnal variations in gene expression. Importantly, we found comparable body weight loss, a similar overall pattern in blood metabolites and hormones, and similar expression patterns of key hepatic fasting genes between the HEP-INTACT and MAC-INTACT mice during fasting (Figure S1J; Table S1), suggesting an overall similar response to fasting in the livers of these two mouse lines. This was supported by the fact that total liver nuclei from HEP-INTACT and MAC-INTACT mice clustered closely together in PCA analyses of the generated RNA-seq data, which further illustrated a strong separation of GFP+ nuclei from the livers of HEP-INTACT and MAC-INTACT mice (Figure S1K).

Transcriptional networks controlling the hepatocyte fasting response

We first evaluated the transcriptional fasting response in hepatocytes and clustered fasting-regulated, hepatocyte-selective genes based on their temporal changes during fasting (Figure 1A). Functional enrichment analysis showed enrichment of gluconeogenic, FAO, and PPAR signaling pathways for the clusters containing genes rapidly induced within 3 h of fasting (i.e., clusters 1 and 2) (Figures 1B, 1C, and S2A). To identify the TFs coordinating these changes, we performed ATAC-seq analyses of GFP+ hepatocyte nuclei (Figures S2B–S2D) and further applied motif response analysis to estimate TF motif activities as well as target enhancers and genes based on integration of ATAC- and RNA-seq data using IMAGE (Madsen et al., 2018) (Figure 1D; Table S2). For fasting-induced genes, these included well-known fasting responsive factors such as Forkhead box protein O1 (FOXO1) and FOXO3 along with GR (Figure 1E). The latter showed a very rapid activation within 3 h of fasting and a dramatic transient decline after 16 h of fasting, which accurately corresponded to the temporal expression profile of the classical GR target gene, *Fkbp5*, in hepatocytes and of serum glucocorticoid levels (Figures 1F–1H). Reassuringly, the predicted GR target enhancers were enriched in liver GR binding as assessed by mining public ChIP-seq data from the CistromeDb and the predicted GR target genes were downregulated in *Nr3c1*^{flox}*; Albumin-Cre*$^{+/-}$ (GR^{HEP}) mice (He et al., 2015) (Figures S2E and S2F), further confirming the validity of this integrative approach.

Fasting dynamics of the liver macrophage transcriptional networks

Next, we investigated the temporal fasting response in macrophages and identified more than 1,000 macrophage-specific, fasting-regulated genes (Figure 2A). Many of these genes encoded for signaling molecules (Figure 2B), indicating that communication with other hepatic cell types could be affected in the fasted mice. Notably, we also identified a cluster of genes progressively repressed during fasting that was strongly enriched for pathways related to the cell cycle (Figure 2B). In line with this, expression of cell cycle and proliferation markers, such as *Mki67*, was dramatically reduced in macrophage nuclei during fasting (Figures 2C and S3A). Accordingly, immunohistochemical analyses showed that both the fraction of KI67+/CLEC4F+ macrophages and the abundance of CLEC4F+ macrophages decreased during a 24-h fast, indicating that fasting decreases the abundance of resident liver macrophages through suppression of macrophage proliferation (Figures 2D, 2E, and S3B).

ATAC-seq analyses of GFP+ macrophage nuclei (Figures S3C–S3E), combined with motif activity response analyses (Figure 2F; Table S3), predicted signal transducer and activator of transcription 2 (STAT2) and several members of the interferon regulatory

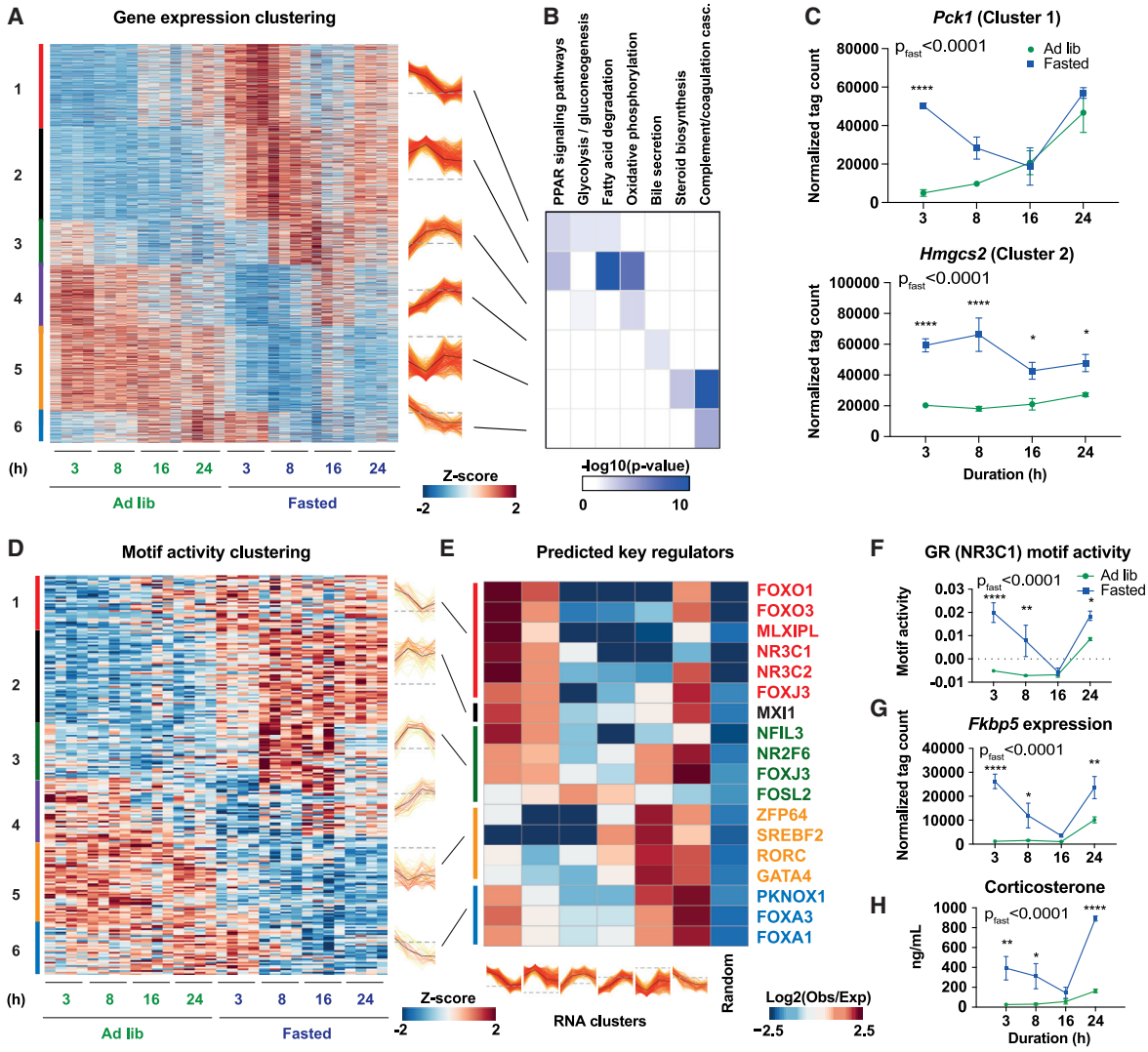

Figure 1. Transcriptional networks controlling the hepatocyte fasting response

(A–G) GFP+ nuclei were obtained from ad libitum fed and fasted HEP-INTACT mice at the indicated time points followed by RNA-seq, ATAC-seq, and IMAGE analyses.

(A) Fuzzy C-means clustering of differentially expressed genes (adjusted $p < 0.05$, membership score > 0.5).

(B) Gene ontology enrichment for the indicated gene clusters.

(C) Expression of (upper) *Pck1* and (lower) *Hmgcs2* (n = 4).

(D) Fuzzy C-means clustering of significantly altered motif activities (adjusted $p < 0.05$, membership score > 0.35).

(E) Enrichment of IMAGE-predicted target genes for indicated TFs in the RNA-seq clusters over a random distribution (observed/expected).

(F) Activity of the GR (encoded by *Nr3c1*) motif 1 (n = 4).

(G) Gene expression of *Fkbp5* (n = 4).

(H) Serum corticosterone levels (n = 4).

(Line plots in A, D, and E) Colored lines, individual genes/motif activities; black lines, cluster mean; dashed gray line, $\log_2$ fold change (log2FC) = 0 or (C and F–H) blue squares (fasted) and green circles (ad libitum fed) represent the mean at each individual time point and vertical lines indicate ± SEM.

Statistical significance was determined using two-way ANOVA with post-hoc Sidak's multiple comparison test between ad libitum fed and fasted mice at the individual time points and indicated by *$p < 0.01$, **$p < 0.01$, ****$p < 0.0001$.

See also Figures S1 and S2.

factor (IRF) family as key regulators of genes that were repressed in macrophages during fasting (Figures 2G and S3F). Notably, also in macrophages, GR appeared to be a key regulator of genes induced early in fasting (Figure 2G), and the motif activity resembled both macrophage-selective GR target gene expression patterns and the levels of glucocorticoids in blood during fasting (Figures 2H–2J). In macrophages, the set of predicted GR target enhancers was highly similar with published macrophage GR cistromes (Figure S3G), and both predicted target enhancers and target genes were very different from those predicted in hepatocytes (Figure S3H) consistent with previous studies on cell-type-specific GR binding and action (John et al., 2011).

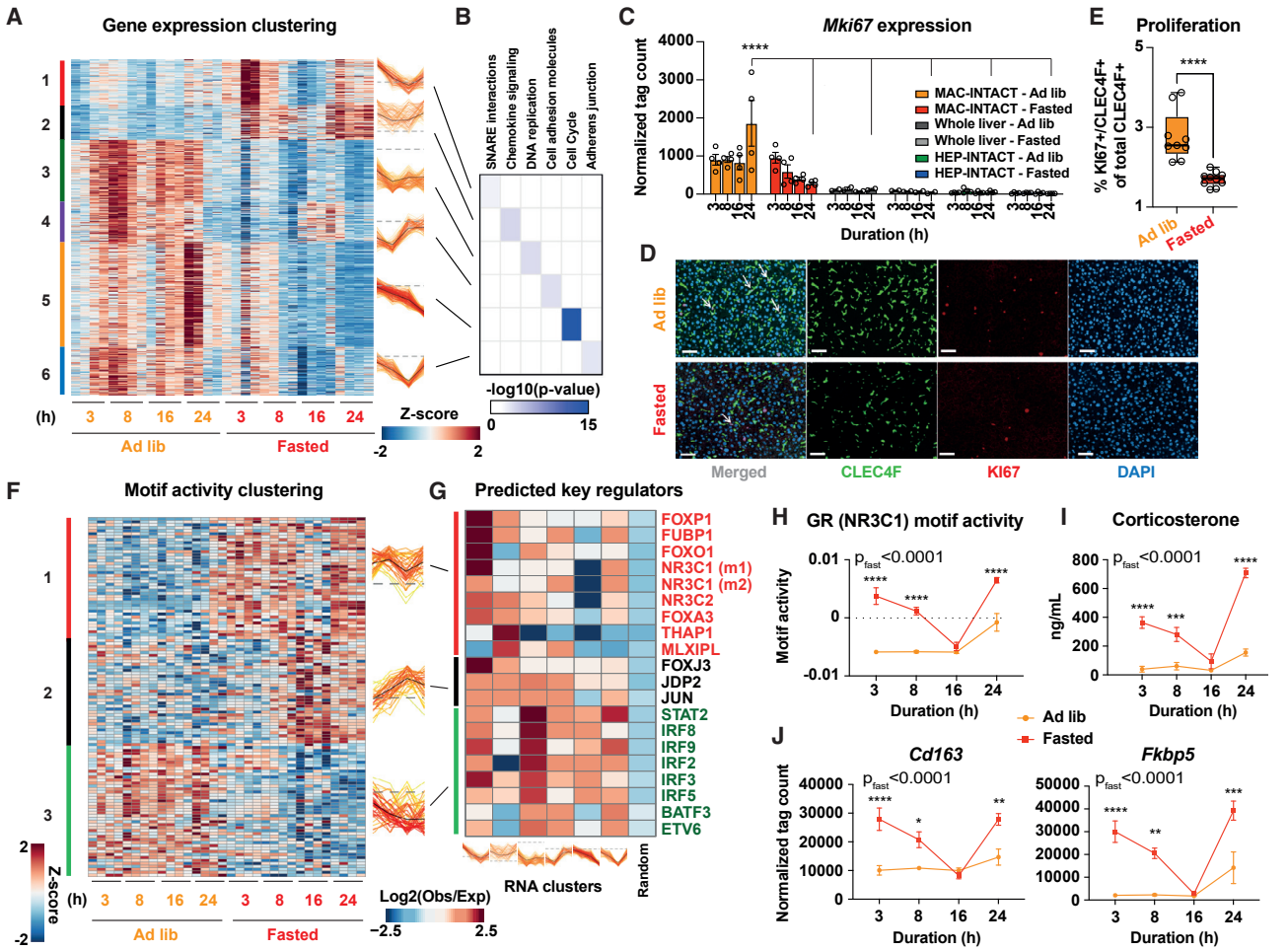

Figure 2. Transcriptional networks controlling the fasting response in liver macrophages

(A–C, F–H, and J) GFP+ nuclei were obtained from ad libitum fed versus fasted MAC-INTACT mice at the indicated time points followed by RNA-seq, ATAC-seq, and IMAGE analyses.

(A) Fuzzy C-means clustering of differentially expressed genes (adjusted $p < 0.05$, membership score > 0.5).

(B) Gene ontology enrichment for the indicated gene clusters.

(C) Expression of *Mki67* in whole liver nuclei (n = 2) and GFP+ nuclei from MAC-INTACT or HEP-INTACT mice (n = 4).

(D) Representative staining of CLEC4F+ (green) and KI67+ cells (red) as well as DAPI+ nuclei in 24-h ad libitum fed (upper) and fasted (lower) B6/N mice. White bars indicate 50 μm.

(E) Quantification of the % of KI67+/CLEC4F+ cells of total CLEC4F+ cells (n = 9–10). Every dot represents one individual mouse. Horizontal line indicates the median and whiskers indicate min to max.

(F) Enrichment of IMAGE-predicted target genes of indicated factors in the RNA-seq clusters over a random distribution (observed/expected).

(G) Fuzzy C-means clustering of significantly altered motif activities (adjusted $p < 0.05$, membership score > 0.35). m1/m2 = motif 1/motif 2.

(H) Activity of the GR (encoded by *Nr3c1*) motif 1 (n = 4).

(I) Serum corticosterone levels (n = 4).

(J) *Cd163* and *Fkbp5* expression (n = 4).

(Line plots in A, F, and G) Colored lines, individual genes/motif activities; black lines, cluster mean; dashed gray line, $\log_2$ fold change (log2FC) = 0. (C) Every dot represents one individual mouse and colored bars indicate mean ± SEM or (H–J) red squares (fasted) and orange circles (ad libitum fed) represent the mean at each individual time point and vertical lines indicate ± SEM.

Statistical significance was determined by (C) two-way ANOVA with Tukey's multiple comparison test (for simplicity only the comparison between nuclei at the 24-h time point is highlighted), (E) unpaired t test, or (H–J) two-way ANOVA with Sidak's multiple comparison test between ad libitum fed and fasted mice at the individual time points and indicated by *$p < 0.05$, **$p < 0.01$, ***$p < 0.001$, ****$p < 0.0001$.

See also Figure S3.

Mutual crosstalk between liver macrophages and hepatocytes during fasting

To explore potential intercellular communication between macrophages and hepatocytes modulating fasting-regulated gene programs in the two populations, we used NicheNet (Browaeys et al., 2020). First, we predicted whether fasting-regulated, hepatocyte-derived ligands had the potential for regulating macrophage-selective gene programs enriched in each of the temporal

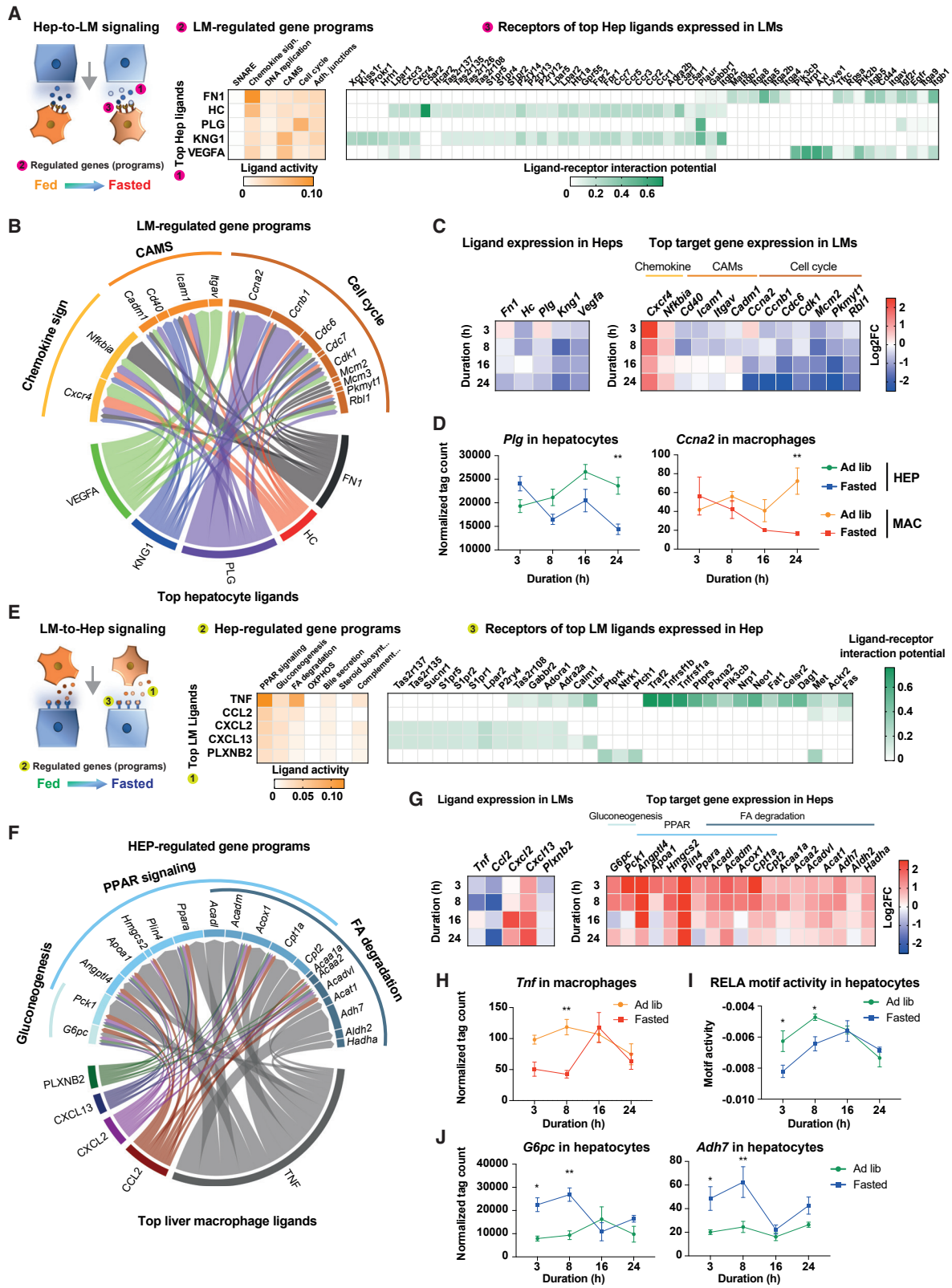

Figure 3. Computational prediction of intercellular communication during fasting

(A and B) NicheNet analysis of upstream ligand-receptor pairs modulating fasting-regulated gene programs in liver macrophages (LM).

(A) NicheNet workflow (left), the activity of top-five predicted upstream hepatocyte ligands (middle), and interaction potential for the predicted receptors in LM (right).

(legend continued on next page)

clusters (Figures 2A and 2B). The top-five prioritized hepatocyte ligands with the highest predicted activity in fasting were particularly associated with chemokine signaling, cell adhesion molecules, and cell cycle, and all had several receptors with high interaction potential on macrophages (Figures 3A and 3B). The expression of the genes encoding the potential ligands in hepatocytes was generally downregulated during fasting, which correlated with the expression pattern of the predicted cell-cycle target genes in macrophages (Figures 3C and 3D).

Next, we asked which macrophage-derived ligands had the potential to regulate fasting-regulated gene programs in hepatocytes (Figures 1A and 1B). Here, the fasting-repressed TNF was predicted to have the highest regulatory potential for genes belonging to PPAR signaling and FA degradation pathways (Figures 3E and 3F). In line with this prediction, the suppression of *Tnf* expression in macrophages temporally coincided with suppression of the motif activity of the downstream TF v-rel avian reticuloendotheliosis viral oncogene homolog A (RELA) in hepatocytes as well as with induction of several key fasting-induced hepatocyte genes (Figures 3G–3J).

Macrophage GR modulates intra-hepatic crosstalk and ketogenesis during fasting

Since our motif activity response analyses pointed toward GR as the main driver of the transcriptional changes that occurred in macrophages during fasting, we next asked whether macrophage GR also plays a role in the intercellular communication to hepatocytes and thereby affects systemic fasting metabolism. To address this question, we used *GR*^{flox}*; LysM-Cre*$^{+/-}$ (GR^{MAC}) mice (Kleiman et al., 2012) and littermate controls (GR^{flox}) and fasted them for 8 h. Notably, GR deficiency in macrophages significantly impaired the induction of blood β-hydroxybutyrate levels (Figure 4A), whereas no significant effects were observed on blood glucose, body/tissue weights, or liver triglycerides (Figures 4B and S4A–S4E). RNA-seq in livers from fasted GR^{MAC} and GR^{flox} mice revealed significant changes for both macrophage and hepatocyte-selective genes (as defined by our INTACT data) as well as a robust overlap with hepatocyte-specific, fasting-regulated genes (Figures S4F–S4H). Functional enrichment analyses revealed that the induction of the hepatocyte-selective FAO/PPAR gene programs during fasting was impaired in GR^{MAC} mice (Figure 4C), which included key ketogenesis and FAO genes, such as *Hmgcs2*, *Cyp4a14*, and *Hadhb* (Figure 4D). We observed no changes in serum nonesterified fatty acid (NEFA) levels or the activation status of hormone-sensitive lipase in the adipose tissue in GR^{MAC} mice (Figures S4I and S4J), suggesting that the observed effects on ketogenesis were not due to altered fatty acid flux from adipose tissue. To further confirm the notion that the impaired ketogenesis was caused by local signaling effects in the liver, we crossed GR^{flox} mice to mice expressing the Cre under direction from the *Clec4f* promoter (Sakai et al., 2019; Scott et al., 2016) ablating GR specifically in the liver resident Kupffer cell (KC) population (Figures S4K–S4M). Indeed, when we fasted these mice (GR^{KC}) and their littermate controls (GR^{flox}) for 8 h, we found a significant impairment in the induction of β-hydroxybutyrate levels as well as a decrease in several of the genes linked to FAO and ketogenesis, similar to the effects observed in the GR^{MAC} mice (Figures 4E, 4F, and S4N). Conditioned medium experiments further confirmed that GR in liver macrophages could promote the expression of FAO and ketogenesis genes in hepatocytes independent of other hepatic cell types (Figures 4G, 4H, and S4O).

We then explored the molecular mechanisms underlying the direct GR-dependent macrophage-to-hepatocyte crosstalk during fasting. To this end, we identified a set of macrophage-selective, fasting-regulated genes annotated to encode for secreted proteins (Xiong et al., 2019) that trended to be regulated in the opposite direction in GR^{MAC} mice (Figures S4P–S4Q). By qPCR, we confirmed that 10 out of 34 of these fasting-regulated secretome genes were significantly altered in the opposite manner in both GR^{MAC} and GR^{KC} mice (Figures 4I, S4R, and S4S), indicating that GR in resident liver macrophages regulates a broad program of secreted factors during the early fasting response. This secretome gene signature included GR-induced genes, such as *Cd163* and *Pla2g7*, and GR-repressed genes, such as *Tnf*, and generally correlated with fasting ketone levels (Figure 4J). TNF was also among the top predicted regulators of various fasting-induced hepatocyte gene programs (Figure 3E), suggesting that its suppression by GR is required for full induction of fasting ketogenesis. In support of this, protein expression of TNF was elevated in fasted GR^{MAC} versus GR^{flox} mice (Figure S4T), and TNF was predicted as the main regulator by NicheNet analysis using predicted fasting-regulated

(B) Predicted interaction links between hepatocyte-derived ligands and their putative LM target genes associated with the indicated KEGG pathway.
(C) Expression change (fasted versus ad lib fed) of the genes encoding the top-five predicted upstream ligands in hepatocyte nuclei (left) and of their top target genes in LM nuclei belonging to the indicated KEGG pathways (right).
(D) Gene expression of *Plg* (left) and *Ccna2* (right) (n = 4) in GFP+ nuclei from ad libitum fed and fasted HEP-INTACT (left) and MAC-INTACT (right) mice at the indicated time points.
(E and F) NicheNet analysis of upstream ligand-receptor pairs regulating the fasting-regulated gene programs in hepatocytes (Hep).
(E) NicheNet workflow (left), the activity of top-five predicted upstream LM ligands (middle), and interaction potential for the predicted hepatocyte receptors (right).
(F) Predicted interaction links between LM-derived ligands and their putative hepatocyte target genes associated with the indicated KEGG pathway.
(G) Expression change (ad lib fed versus fasted) of the genes encoding the top-five predicted upstream ligands in LM nuclei (left) and of their top target genes in hepatocyte nuclei belonging to the indicated KEGG pathways (right).
(H–J) Gene expression of (H) *Tnf* and (J) *G6pc* and *Adh7* as well as (I) motif activity of RELA (n = 4) in GFP+ nuclei from ad libitum fed and fasted (H) MAC-INTACT and (I and J) HEP-INTACT mice.
(D and H–J) Red squares (fasted) and orange circles (ad libitum fed) indicating GFP+ nuclei from MAC-INTACT mice or blue squares (fasted) and green circles (ad libitum fed) indicating GFP+ nuclei from HEP-INTACT mice represent the mean at each individual time point and vertical lines indicate ± SEM.
Statistical significance was determined by two-way ANOVA with Sidak's multiple comparison test between ad libitum fed and fasted mice at the individual time points and indicated by *p < 0.05, **p < 0.01.

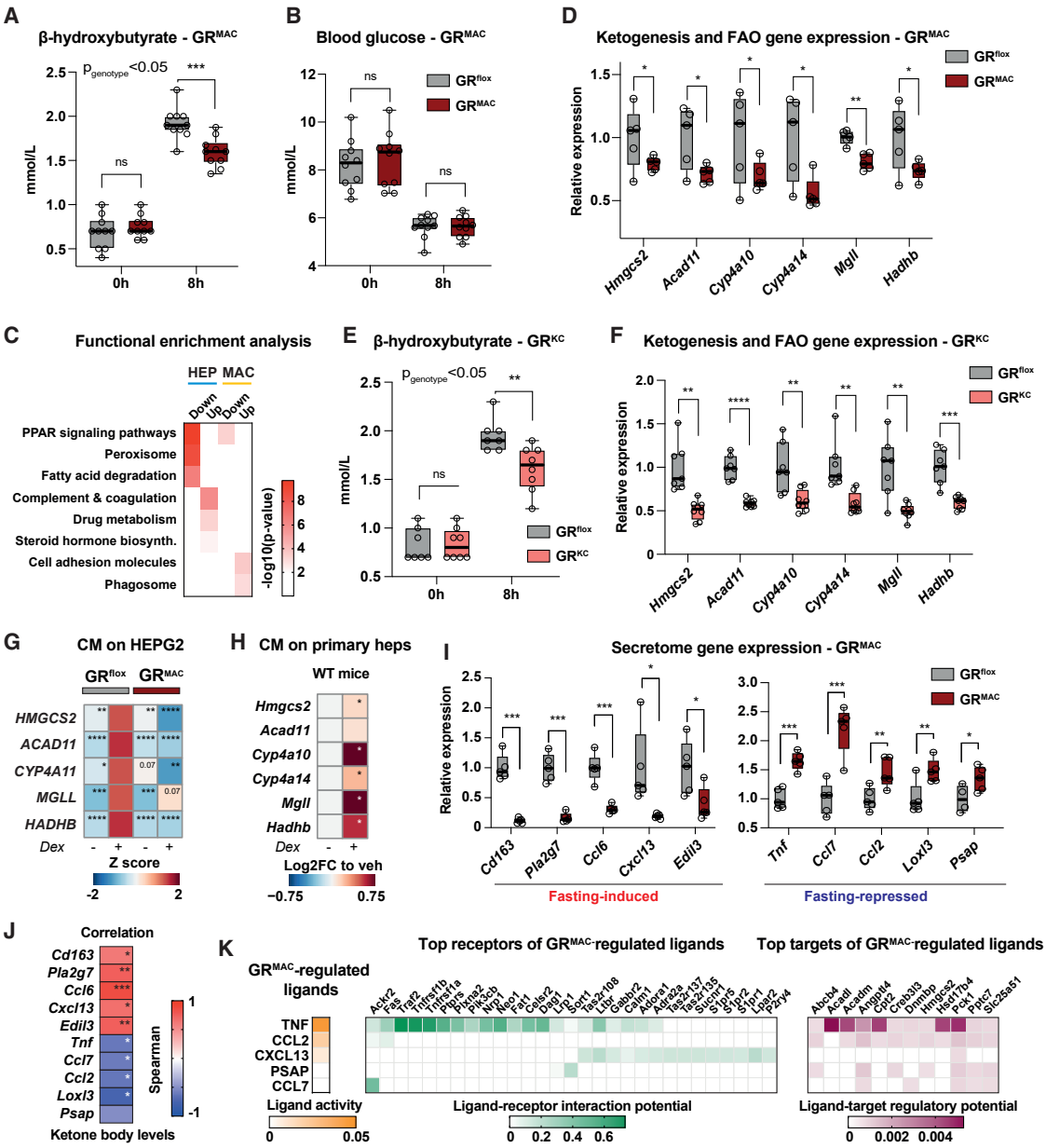

Figure 4. Macrophage GR modulates intrahepatic crosstalk and ketogenesis during fasting

(A and B) Blood levels of (A) β-hydroxybutyrate and (B) glucose in GR^{MAC} versus GR^{flox} mice fasted for 8 h (n = 10). Every dot represents one individual animal.

(C) Functional enrichment analyses of significantly regulated genes identified in Figure S4F divided into hepatocyte and macrophage-selective genes (as defined by INTACT RNA-seq data).

(D) Expression (qPCR) of ketogenesis and FAO genes in the livers of GR^{MAC} versus GR^{flox} mice (n = 5). Every dot represents one individual animal.

(E) Blood levels of β-hydroxybutyrate in GR^{KC} versus GR^{flox} mice fasted for 8 h (n = 7–8).

(F) Expression (qPCR) of ketogenesis and FAO genes in the livers of GR^{KC} versus GR^{flox} mice (n = 7–8). Every dot represents one individual animal.

(G) Row-scaled median expression (qPCR) in HEPG2 hepatocytes treated with liver-macrophage-conditioned medium (LM-CM) (cultured with vehicle (-) or dexamethasone [Dex]) obtained from GR^{flox} or GR^{MAC} mice (n = 6).

(H) Log2FC (Dex versus veh CM) in mean expression (qPCR) in primary hepatocytes treated with LM-CM obtained from WT B6/J mice (n = 5).

(I) Expression (qPCR) of indicated secretome genes in GR^{MAC} versus GR^{flox} mice fasted for 8 h (n = 5). Every dot represents one individual animal.

(J) Spearman correlation coefficient between the expression (qPCR) of indicated GR-regulated secretome genes and ketone blood levels in GR^{flox} and GR^{MAC} mice fasted for 8 h.

(K) NicheNet analysis of upstream ligand-receptor pairs regulating early fasting-induced genes repressed in the livers of GR^{MAC} versus GR^{flox} mice. Activity of the predicted upstream LM-derived ligands (left), interaction potential for the predicted hepatocyte receptors (middle), and the regulatory potential for the predicted top target genes (right) expressed by hepatocytes associated with each LM ligand.

(A, B, D–F, and I) Horizontal line indicates the median, and whiskers indicate min to max.

(legend continued on next page)

macrophage ligands and hepatocyte target genes significantly altered in the GR^{MAC} mice (Figure 4K).

Macrophage GR modulates ketogenesis in endotoxemia

To explore whether macrophage GR modulates ketone body levels in conditions other than fasting, we investigated the response of GR^{MAC} mice to endotoxemia, where macrophage GR (Bhattacharyya et al., 2007; Kleiman et al., 2012) and ketogenesis (Paumelle et al., 2019; Van Wyngene et al., 2020; Wang et al., 2016) both have been shown to promote survival. We therefore administered GR^{MAC} and GR^{flox} mice with a single intraperitoneal injection of lipopolysaccharide (LPS) and followed the mice for an 8-h period (Figures S5A–S5G). Indeed, we found an impaired induction of blood β-hydroxybutyrate levels in GR^{MAC} mice (Figure S5A), which was accompanied by changes of the macrophage secretome gene signature and of FAO/ketogenesis genes in hepatocytes highly similar to those observed in fasted GR^{MAC} mice (Figures S5H–S5J). Thus, the regulation of ketogenesis by macrophage GR appears to be a more general regulatory principle in metabolic health and disease.

GR in liver macrophages promotes cooperative GR- and PPARα-dependent gene expression in hepatocytes

Next, we asked which TFs in hepatocytes responded to the GR-dependent modulation of the macrophage secretome. Epigenetic landscape *in silico* deletion analysis (Qin et al., 2020) found that enhancers near hepatocyte-selective, GR^{MAC}-repressed genes were enriched for both binding and motifs of GR and PPARα (Figures 5A and 5B), suggesting that macrophage GR signals to these two NRs in hepatocytes. In further support of this notion, hepatocyte-selective genes with decreased expression in GR^{MAC} mice were generally repressed in mice with hepatocyte-specific deletion of GR or PPARα and induced by treatment with their respective ligands dexamethasone (Dex) or fenofibrate (Figure S6A) (He et al., 2015; Montagner et al., 2016). Notably, genes repressed both in mice with hepatocyte-specific deletion of GR or PPARα were preferentially repressed in GR^{MAC} mice compared with genes repressed in only one of these models (Figure 5C), suggesting that GR in macrophages promotes cooperativity between GR and PPARα in hepatocytes. To further explore this, we investigated the response of hepatocyte-selective, GR^{MAC}-repressed genes to ligand activation of GR and PPARα alone or in combination in primary hepatocyte cultures (Ratman et al., 2016). Indeed, this gene program was robustly activated by coactivation of these two NRs in hepatocytes, whereas the response to individual ligand was less pronounced (Figure 5D). Moreover, genes synergistically activated by the combined treatment displayed a markedly higher degree of overlap with hepatocyte-selective, GR^{MAC}-repressed genes, compared with genes induced by only one ligand and cooperatively induced genes (Figure 5E). Mechanistically, loss of macrophage GR did not alter protein levels of PPARα or GR in whole liver lysates, and circulating corticosterone levels were unaltered in GR^{MAC} mice (Figures S6B and S6C). This further supported the notion that changes in the FAO and ketogenesis gene programs were consequences of local signaling events in the liver, post-translationally controlling the activity of these NRs in hepatocytes. Interestingly, we observed decreased nuclear localization of GR but not PPARα in livers of GR^{MAC} mice (Figure 5F) and further confirmed that GR was less abundant in HNF4α+ hepatocyte nuclei from GR^{MAC} compared with GR^{flox} mice (Figures 5G and S6D), thus indicating direct crosstalk between GR in macrophages and GR in hepatocytes during fasting.

TNF selectively represses PPARα target genes highly dependent on hepatocyte GR

Since TNF was predicted as the main mediator of the macrophage-to-hepatocyte crosstalk observed in the GR^{MAC} mice, we next investigated the effects of TNF in primary hepatocytes co-treated with PPARα and GR ligands. Here, we found repression of several of the key fasting-induced genes shown to be repressed in the GR^{MAC} mice even at very low TNF doses (Figure 6A). By RNA-seq analyses, we further demonstrated an overall repressive effect by TNF on the hepatocyte-selective gene program found to be repressed in the GR^{MAC} mice (Figure S6E). Furthermore, TNF-repressed genes were robustly activated by GR ligand alone or the combinatorial PPARα/GR ligand treatment of primary hepatocytes, whereas the PPARα ligand alone had a very limited effect on these genes (Ratman et al., 2016) (Figure 6B). To further explore this observation, we treated primary hepatocytes for 8 h with GR and PPARα ligands alone or in combination to initially determine how 14 different PPARα target genes involved in FAO and ketogenesis depended on GR coactivation under our specific conditions (Figures 6C, S6F, and S6G). We then explored which of these genes were most sensitive to an 8-h treatment of primary hepatocytes with TNF or, as a control, the related inflammatory cytokine IL1β, which has previously been shown to inhibit PPARα activity (Stienstra et al., 2010). Using this setup, we did not observe significant effects on *Ppara* expression with neither IL1β nor TNF treatment (Figure S6H), suggesting that any observed effects were consequences of posttranscriptional signaling events. Interestingly, IL1β broadly repressed all 14 PPARα target genes, including genes with a low GR dependency index, such as *Pdk4*, whereas TNF affected only genes highly dependent on GR coactivation, such as *Hmgcs2* and *Cyp4a14* (Figures 6D and 6E). Thus, TNF repressed only the subset of PPARα target genes that were co-activated by GR, and in line with this, we found that TNF attenuated ligand-induced GR nuclear translocation in primary hepatocytes (Figures 6F and 6G). This resemblance with our observations of decreased nuclear translocation of hepatocyte GR in the GR^{MAC} mice indicates that macrophage GR promotes nuclear translocation of hepatocyte GR and coactivation of selected FAO and ketogenesis genes at least in part via suppression of local TNF signaling during fasting.

Statistical significance was determined by (A, B, E, and G) two-way ANOVA with post hoc (A, B, and E) Sidak's multiple comparison test (GR^{MAC}/GR^{KC} versus littermate GR^{flox} mice) at the individual time points or (G) Tukey's multiple comparison test between all conditions (indicated is significance level to HEPG2 cells treated with Dex LM-CM from GR^{flox} mice), (D, F, and I) multiple t test with FDR correction, (H) paired ratio t test, or (J) unpaired t test and indicated by *p < 0.05, **p < 0.01, ***p < 0.001, ****p < 0.0001 or when corrected for multiple testing by *q < 0.05, **q < 0.01, ***q < 0.001, ****q < 0.0001; ns, not significant
See also Figures S4 and S5.

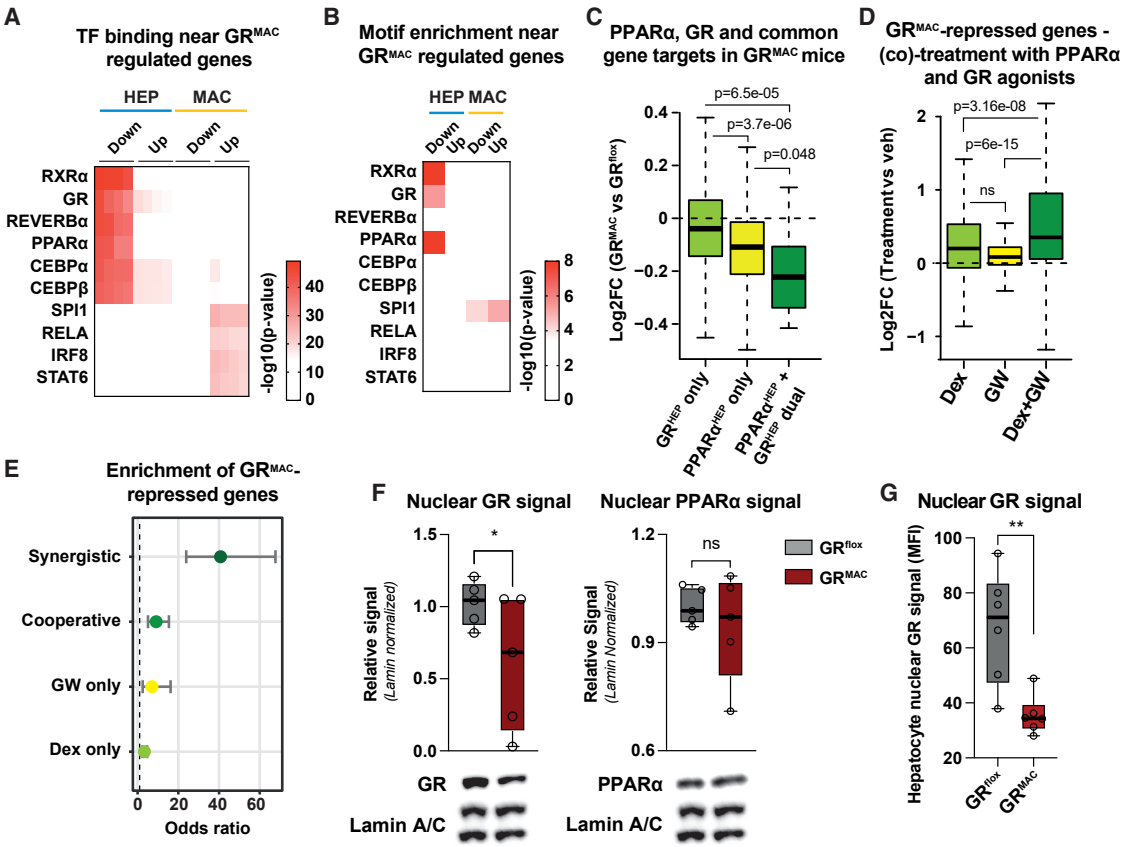

Figure 5. GR in liver macrophages promotes cooperative GR and PPARα target gene activation in hepatocytes

(A and B) LISA enrichment analysis of (A) TF binding (ChIP-seq from CistromeDB) and (B) motifs of the TFs depicted in (A) near hepatocyte or macrophage-selective genes significantly regulated in GR^{MAC} versus GR^{flox} mice (as defined in Figure S4F).

(C) Log2FC in whole liver expression in GR^{MAC} versus GR^{flox} for genes downregulated only by knockout of GR (261 genes), only by knockout of PPARα (298 genes), or by both knockout of PPARα and GR (22 genes) (adjusted $p < 0.05$) identified by microarray analysis of livers from $PPAR\alpha^{HEP}$ versus $PPAR\alpha^{flox}$ and GR^{HEP} versus GR^{flox} mice.

(D) Log2FC in the expression of hepatocyte-selective, downregulated genes in GR^{MAC} versus GR^{flox} (as defined in Figure S4F) in dexamethasone (Dex) versus vehicle (Veh)-treated (light green), GW7647 (GW) versus Veh-treated (yellow), and dual Dex/GW versus Veh-treated (dark green) primary hepatocytes.

(E) Enrichment (indicated by odds ratio) of hepatocyte-selective, downregulated genes in GR^{MAC} versus GR^{flox} mice (as defined in Figure S4F) for genes induced in primary hepatocytes by Dex only (light green) and GW only (yellow) as well as genes cooperatively (green) and synergistically (dark green) induced by Dex and GW co-treatment.

(F) Protein expression of nuclear GR (left) and nuclear PPARα (right) in GR^{flox} and GR^{MAC} mice. Protein expression was normalized to Lamin A/C nuclear expression. The western blots depicted are pools of individual mice (n = 5), and the Lamin A/C blot is duplicated due to the use of the same membrane for detection of GR, PPARα, and Lamin A/C.

(G) Quantification of hepatocyte GR nuclear signal (average nuclear median fluorescence intensity [MFI]) as determined in double DAPI+/ HNF4α+ nuclei from livers of GR^{flox} and GR^{MAC} mice.

(C, D, F, and G) Horizontal line indicates the median, and (C and D) whiskers indicate 1.5× IQR or (F and G) min-to-max. (E) Circle indicates odds ratio with a 95% confidence interval indicated. Statistical significance was determined by (C) Kruskal-Wallis' one-way analysis and (D) Friedman's test with post hoc Dunn's multiple comparison test between conditions or (F and G) unpaired t test and indicated by exact p value or *$p < 0.05$, **$p < 0.01$; ns, not significant.

See also Figure S6.

GR in liver macrophages is required for hepatocyte GR-dependent fasting ketogenesis

Finally, since our data suggested that macrophage GR is required for activation of GR in hepatocytes and full activation of fasting ketogenesis, we hypothesized that depletion of hepatocyte GR mice should phenocopy the impaired fasting ketogenesis in GR^{MAC} mice, whereas loss of GR in both populations should be redundant compared with depletion in just one population. To investigate this, we administered GR^{MAC} and GR^{flox} mice with an adeno-associated viral vector (AAV) driving Cre recombinase expression from the hepatocyte-specific LP1 promoter (Kulozik et al., 2011; Nathwani et al., 2006; Rose et al., 2011), to achieve GR KO in macrophages (GR^{MAC}), hepatocytes (GR^{HEP}), or in both of these cell populations (GR^{DKO}) (Figure 7A). As expected, we observed decreased whole liver expression of *Nr3c1* only in GR^{HEP} and GR^{DKO} mice (Figure S7A) and effects on the macrophage secretome gene program predominantly in GR^{MAC} and GR^{DKO} mice (Figures S7B and S7C), whereas *Ppara* levels were not changed in any of the groups (Figure S7A). Indeed, loss of GR in hepatocytes decreased fasting-serum

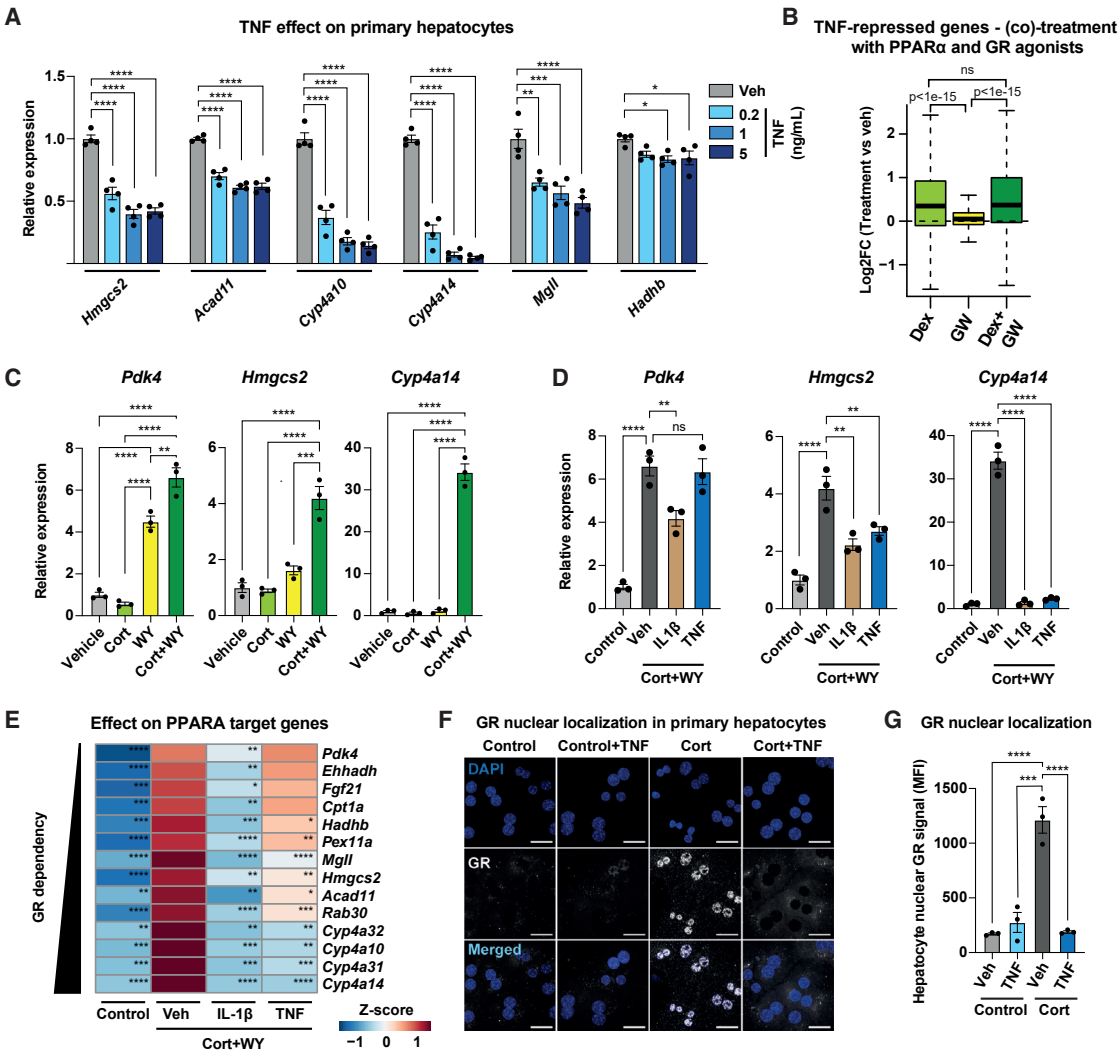

Figure 6. TNF attenuates hepatocyte GR nuclear translocation and induction of cooperatively activated GR/PPARα target genes in hepatocytes

(A) Expression (qPCR) of the indicated genes in primary hepatocytes treated for 8 h with vehicle or TNF (n = 4).

(B) Log2FC in the expression of genes downregulated in TNF versus vehicle (Veh)-treated primary hepatocytes in dexamethasone (Dex) versus Veh-treated (light green), GW7647 (GW) versus Veh-treated (yellow), and dual Dex/GW versus Veh-treated (green) primary hepatocytes.

(C) Expression (qPCR) of *Pdk4*, *Hmgcs2*, and *Cyp4a14* in primary hepatocytes treated for 8 h with vehicle, corticosterone (Cort), WY-14643 (WY), or a combination of Cort+WY.

(D) Expression (qPCR) of *Pdk4*, *Hmgcs2*, and *Cyp4a14* in primary hepatocytes treated for 8 h with control or a combination of Cort+WY together with vehicle (Veh), IL1β, or TNF.

(E) Row-scaled mean expression (qPCR) of indicated PPARα target genes in primary hepatocytes treated for 8 h with control or a combination of Cort+WY together with vehicle (Veh), IL1β, or TNF.

(F) Representative stainings showing GR+ (white) and DAPI+ (blue) nuclei in primary hepatocytes treated for 1 h with vehicle or a combination of Cort+WY with or without TNF. The merged picture shows an overlay of the two stainings. White scale bar, 25 μm.

(G) Quantification of GR nuclear signal (average nuclear median fluorescence intensity [MFI]) as determined in DAPI+ nuclei from primary hepatocytes treated as described in (F) (n = 3).

(A. C, D, and G) Every dot represents primary hepatocytes isolated from one individual mouse and colored bars represent mean and vertical lines indicate ± SEM or (B) horizontal line indicates the mean and whiskers indicate 1.5× IQR.

Statistical significance was determined by (A, C, D, and E) one-way ANOVA with post-hoc (A, D, and E) Dunnett's multiple comparison test between (A) vehicle and the TNF treatment conditions and (D and E) the treatment with Cort+WY+Veh and the other conditions, or (C) Tukey's multiple comparison test between all conditions, (B) Friedman's test with post hoc Dunn's multiple comparison test between conditions, or (G) two-way ANOVA with post hoc Tukey's multiple comparison test between all conditions and indicated by exact p value or *p < 0.05, **p < 0.01, ***p < 0.001, ****p < 0.0001; ns, not significant.

See also Figure S6.

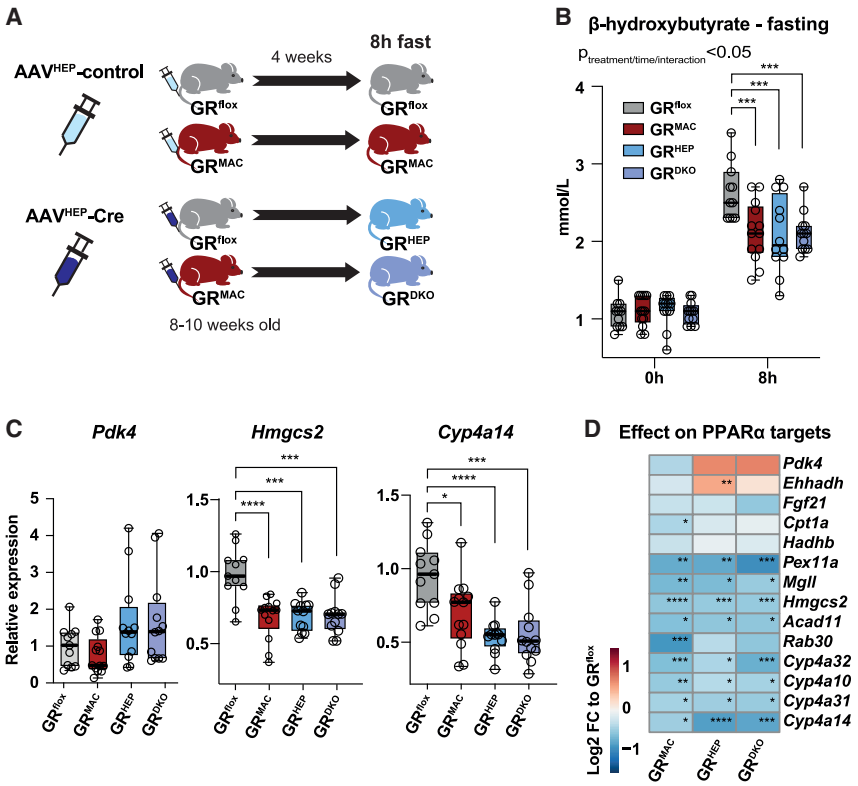

Figure 7. GR in liver macrophages and hepatocytes collaborate to enhance fasting ketogenesis

(A) Eight- to ten-week-old GR^{flox} and GR^{MAC} mice were injected with AAVs encoding control (AAV^{HEP}-control) or Cre recombinase (AAV^{HEP}-Cre) resulting in GR^{flox}, GR^{HEP} (i.e., GR^{flox} mice with AAV-mediated knockdown of *Nr3c1* in hepatocytes), GR^{MAC}, and GR^{DKO} (i.e., GR^{MAC} mice with additional AAV-mediated abrogation of *Nr3c1* expression in hepatocytes). Four weeks post-injection, mice were fasted for 8 h.

(B) Blood levels of β-hydroxybutyrate (n = 11–13).

(C) Whole-liver expression (qPCR) of *Pdk4* (left), *Hmgcs2* (middle), and *Cyp4a14* (right) (n = 11–13).

(D) Log2FC of mean whole-liver expression (qPCR) (GR^{MAC}/GR^{HEP}/GR^{DKO} versus GR^{flox} mice) for the indicated genes.

(B and C) Every dot represents one individual mouse. Horizontal line indicates the median and whiskers indicate min-to-max.

Statistical significance was determined by (B) two-way ANOVA with post hoc Tukey's multiple comparison test between conditions at the individual time points or (C and D) one-way ANOVA with post hoc Tukey's multiple comparison test between conditions. Significance level compared with GR^{flox} is displayed in (D) and indicated by exact p value or *p < 0.05, ***p < 0.001, ****p < 0.0001.

See also Figure S7.

ketone levels to a similar extent as loss of GR in macrophages, whereas there was no further impairment in GR^{DKO} mice (Figure 7B). Similarly, GR was generally required in both cell types to activate TNF-sensitive FAO/ketogenesis genes, such as *Cyp4a14* and *Hmgcs2*, above the levels observed in GR^{DKO} mice (Figures 7C and 7D). In contrast, TNF-insensitive genes, such as *Pdk4* and *Ehhadh*, were generally not repressed in GR^{MAC} mice and particularly not in GR^{HEP} mice (Figures 7C and 7D). Taken together, our data demonstrate that GR in resident liver macrophages is required for repression of TNF and activation of GR nuclear translocation in hepatocytes to enhance fasting-induced ketogenesis via cooperative activation of GR- and PPARα-dependent FAO/ketogenesis genes in hepatocytes.

DISCUSSION

The liver plays a central role in systemic metabolic homeostasis in mammals by switching between catabolic and anabolic carbohydrate and lipid metabolism in response to circulating endocrine cues. Whereas the regulation of these processes in the parenchymal hepatocytes is well characterized, less is known about how nonparenchymal cells such as liver macrophages contribute to metabolic homeostasis during fasting. In our study, we propose that transcriptional programs of hepatocytes and macrophages during fasting are shaped by mutual crosstalk, including modulation of several macrophage-derived, fasting-regulated cytokines predicted to impact on FAO and ketogenesis gene programs in hepatocytes. Interestingly, macrophage GR was required for modulation of these macrophage secretome genes and activation of ketogenesis during fasting. Mechanistically, loss of GR in macrophages disrupted a gene program synergistically regulated by GR and PPARα in hepatocytes, most likely via decreased nuclear localization of hepatocyte GR. This appears to be caused by increased TNF expression in GR^{MAC} mice since GR nuclear localization in primary hepatocyte cultures was highly sensitive to this cytokine. Whereas previous studies have reported mutual inhibition of GR and TNF-activated RELA transcriptional activities via competition for cofactors (Dendoncker et al., 2019; Gerber et al., 2021; Schmidt et al., 2016), this is to our knowledge the first report of TNF controlling nuclear translocation of GR. Further studies are needed to identify the pathways activated by TNF to promote nuclear exclusion of GR specifically in hepatocytes. Physiologically, the contribution of macrophage and hepatocyte GR to fasting ketogenesis adds to the previously described contribution of GR in adipocytes to fasting ketogenesis via induction of adipose tissue lipolysis (Mueller et al., 2017) and raises the possibility that cell-type-specific actions of GR across multiple tissues and cell types combine to a hitherto unappreciated importance of GR for fasting ketogenesis and energy homeostasis.

The intriguing capacity of resident liver macrophages to control hepatocyte function during periods of fasting may also have implications during obesity, where the function of liver macrophages has been well documented (Huang et al., 2010; Lanthier et al., 2010; Stienstra et al., 2010) and where intervention with fasting and caloric restriction regimens has proven efficient. Indeed, perturbation of hepatocyte ketogenesis and mitochondrial acetoacetate metabolism in resident macrophages was recently shown to accelerate diet-induced hepatic fibrosis (Puchalska et al., 2019). Thus, macrophage-GR-promoted ketogenesis in hepatocytes may feedback to shape an antifibrotic

metabolic profile of resident macrophages. In this context, the suppression of resident macrophage proliferation observed upon prolonged fasting and possibly mediated via repression of hepatocyte-derived ligands, predicted to regulate cell-cycle genes in macrophages, may also be important. Interestingly, hepatocyte plasminogen, which had the highest predicted regulatory activity for macrophage-associated cell-cycle genes, was also among a panel of secreted factors, the fasting-regulation of which was recently proposed to mediate the reduction of the circulating monocyte pool by the hepatic energy sensors AMPK and PPARα (Jordan et al., 2019). Thus, extensive bidirectional crosstalk with hepatocytes may affect the abundance and metabolic state of liver macrophages to contribute to the effectiveness of fasting and caloric restriction regimens as interventions for chronic inflammatory conditions, such as metabolic-associated fatty liver disease.

Several recent studies have reported essential roles of ketogenesis for tissue tolerance and survival during bacterial infections (Paumelle et al., 2019; Van Wyngene et al., 2020; Wang et al., 2016); thus, it is also tempting to speculate that the macrophage-to-hepatocyte GR axis has evolved to provide the immune system direct local control of ketogenesis during infections. Indeed, we observed impaired induction of ketogenesis in GR^{MAC} mice in response to LPS administration, possibly contributing to the previously reported impaired survival of these mice in response to LPS-induced endotoxemia (Bhattacharyya et al., 2007; Kleiman et al., 2012). High levels of inflammatory cytokines, such as TNF, have previously been proposed to suppress ketogenesis in the context of infection (Beylot et al., 1992; Pailla et al., 1998). Our findings extend this observation and indicate that this response is actively counteracted by macrophage GR, which thereby has the capacity to protect hepatic ketogenesis during endotoxemia.

Whereas TNF is well described under inflammatory conditions, it has to our knowledge not been described in the context of the feeding to fasting transition in healthy subjects with low circulating levels of TNF. Combined with the previously described lipogenic (Feingold and Grunfeld, 1987) and mitogenic (Peng et al., 2018) effects of TNF on hepatocytes, our results now indicate that repression of TNF by GR represents a novel local macrophage-derived signal that facilitates a switch from anabolic metabolism in the fed state to catabolic metabolism upon fasting. A necessity of reduced basal macrophage cytokine expression for full induction of ketogenesis would expand the concept of homeostatic or physiological inflammation to local control of hepatic metabolism via suppression of hepatocyte glucocorticoid resistance.

Limitations of study

In this study, we highlight secreted molecules potentially responsible for the impact of liver macrophage GR on fasting ketogenesis. Based on *in vitro* observations, we suggest that suppression of local TNF signaling contributes to the induction of fasting ketogenesis in hepatocytes by permitting nuclear translocation of hepatocyte GR. To formally prove this, one would need to rescue the ketogenesis defect caused by macrophage GR deficiency, by perturbing TNF in liver macrophages or components of the TNF signaling pathways acting upstream of GR in hepatocytes. Furthermore, the preferential suppression of genes synergistically activated by GR and PPARα upon loss of macrophage GR supports a model involving additional parallel signals to PPARα. Thus, fasting-induced, highly macrophage-GR-dependent factors, such as CD163 and PLA2G7, may also contribute to the decreased fasting ketogenesis in GR^{MAC} mice. Further *in vivo* studies are needed to determine the relative contributions of these macrophage-GR-modulated factors and their individual mechanisms of action upstream of hepatocyte GR and PPARα.

STAR★METHODS

Detailed methods are provided in the online version of this paper and include the following:

- KEY RESOURCES TABLE
- RESOURCE AVAILABILITY
  - Lead contact
  - Materials availability
  - Data and code availability
- EXPERIMENTAL MODEL AND SUBJECT DETAILS
  - Animal models and experiments
  - Isolation and culture of primary cells and cell lines
- METHOD DETAILS
  - Adeno-associated virus (AAV) generation
  - Isolation of GFP-tagged nuclei
  - Serum, plasma and liver assays
  - Histology and image analyses
  - Protein analysis
  - RNA isolation and quantitative PCR analysis
  - RNA-seq library construction and sequencing
  - ATAC-seq library construction and sequencing
  - Processing and analyses of INTACT RNA-seq data
  - NicheNet ligand activity and secretome analyses
  - Processing and analyses of bulk RNA-seq data
  - Epigenetic landscape *in silico* deletion analysis
  - Processing and analyses of ATAC-seq data
  - TF motif activity, target sites and genes
  - Analyses of public datasets
- QUANTIFICATION AND STATISTICAL ANALYSIS
  - Statistical analyses

SUPPLEMENTAL INFORMATION

Supplemental information can be found online at https://doi.org/10.1016/j.cmet.2022.01.004.

ACKNOWLEDGMENTS

We thank Alexander Rauch, Luke Harrison, Maude Giroud, and Pauline Morigny for guidance and discussions and Prof. M. Vujić Spasić for kindly providing HepG2 cells. We acknowledge the team of technicians at IDC for assistance with mouse work as well as E. Graf from HMGU and R. Nielsen from SDU for help with sequencing. We thank the Ulm University Centre for Translational Imaging MoMAN and Core Facility Confocal and Multiphoton Microscopy for the support. The graphical abstract was created with BioRender.com. The microscope SP8 Leica was funded by the German Research Foundation (DFG) through grant 91BGG INST 381/39-1. This work was financially supported by grants from the Deutsche Forschungsgemeinschaft (DFG, German Research Foundation) through the Collaborative Research Center (CRC) 1118, project number 236360313 to S.H. and P.N.; through CRC 1052, project number 209933838 (Project B1) to M.B.; through CRC 1149, project number 251293561 (Project C02) to J.T.; and through project number Tu 220/13 to J.T. The work was also financially supported by grants from the

Danish National Research Foundation (DNRF grant no. 141 to ATLAS) and the Novo Nordisk Foundation (NNFOC150019050) to S.F.S. A.L. was supported by fellowships from the Novo Nordisk Foundation (NNF16OC0020742), the Danish Independent Research Council | Medical Sciences (DFF-6110-00265), an EMBO Long-Term Fellowship (ALTF 897-2015), and a DZD grant NEXT. G.C. was supported by EFSD/Lilly, a Bausteingrant from the Medical Faculty of Ulm University, and ProtrainU grant from Ulm University.

AUTHOR CONTRIBUTIONS

Conceptualization, S.F.S., A.L., and S.H.; methodology, A.L., S.F.S., and G.C.; formal analyses, A.L., S.F.S., G.C., Y.K., A.B., and A.F.; investigation, A.L., S.F.S., G.C., U.S., J.H., R.S., Y.K., A.J.A., K.K.C., F.F.T., and A.M.; resources, A.L., S.F.S., G.C., J.H., A.S., N.R., M.S., T.S., A.F., N.M., M.B., P.N., J.S., N.J.F., A.Z., J.T., and S.H.; writing – original draft, A.L., S.F.S., G.C., and S.H.; writing – review & editing, A.L., S.F.S., G.C., J.T., and S.H.; visualization, A.L.; supervision, S.F.S., N.J.F., A.Z., J.T., and S.H.; project administration, A.L., S.F.S, G.C., J.T., and S.H.; funding acquisition, A.L., S.F.S., G.C., J.T., and S.H.

DECLARATION OF INTERESTS

The authors declare no competing interests.

Received: March 12, 2021
Revised: September 30, 2021
Accepted: January 11, 2022
Published: February 3, 2022

REFERENCES

Beylot, M., Vidal, H., Mithieux, G., Odeon, M., and Martin, C. (1992). Inhibition of hepatic ketogenesis by tumor necrosis factor-alpha in rats. Am. J. Physiol. *263*, E897–E902.

Bhattacharyya, S., Brown, D.E., Brewer, J.A., Vogt, S.K., and Muglia, L.J. (2007). Macrophage glucocorticoid receptors regulate toll-like receptor 4-mediated inflammatory responses by selective inhibition of p38 MAP kinase. Blood *109*, 4313–4319.

Bourke, C.D., Berkley, J.A., and Prendergast, A.J. (2016). Immune dysfunction as a cause and consequence of malnutrition. Trends Immunol *37*, 386–398.

Browaeys, R., Saelens, W., and Saeys, Y. (2020). NicheNet: modeling intercellular communication by linking ligands to target genes. Nat. Meth. *17*, 159–162.

Clausen, B.E., Burkhardt, C., Reith, W., Renkawitz, R., and Förster, I. (1999). Conditional gene targeting in macrophages and granulocytes using LysMcre mice. Transgen. Res. *8*, 265–277.

Deal, R.B., and Henikoff, S. (2010). A simple method for gene expression and chromatin profiling of individual cell types within a tissue. Dev. Cell *18*, 1030–1040.

Dendoncker, K., Timmermans, S., Vandewalle, J., Eggermont, M., Lempiäinen, J., Paakinaho, V., Van Hamme, E., Dewaele, S., Vandevyver, S., Ballegeer, M., et al. (2019). TNF-alpha inhibits glucocorticoid receptor-induced gene expression by reshaping the GR nuclear cofactor profile. Proc. Natl. Acad. Sci. USA *116*, 12942–12951.

Dobin, A., Davis, C.A., Schlesinger, F., Drenkow, J., Zaleski, C., Jha, S., Batut, P., Chaisson, M., and Gingeras, T.R. (2013). STAR: ultrafast universal RNA-seq aligner. Bioinformatics *29*, 15–21.

Feingold, K.R., and Grunfeld, C. (1987). Tumor necrosis factor-alpha stimulates hepatic lipogenesis in the rat in vivo. J. Clin. Invest. *80*, 184–190.

Ganeshan, K., Nikkanen, J., Man, K., Leong, Y.A., Sogawa, Y., Maschek, J.A., Van Ry, T., Chagwedera, D.N., Cox, J.E., and Chawla, A. (2019). Energetic trade-offs and hypometabolic states promote disease tolerance. Cell *177*, 399–413.e12.

Gao, G.P., Alvira, M.R., Wang, L., Calcedo, R., Johnston, J., and Wilson, J.M. (2002). Novel adeno-associated viruses from rhesus monkeys as vectors for human gene therapy. Proc. Natl. Acad. Sci. USA *99*, 11854–11859.

Gerber, A.N., Newton, R., and Sasse, S.K. (2021). Repression of transcription by the glucocorticoid receptor: a parsimonious model for the genomics era. J. Biol. Chem. *296*, 100687.

Godoy, P., Hewitt, N.J., Albrecht, U., Andersen, M.E., Ansari, N., Bhattacharya, S., Bode, J.G., Bolleyn, J., Borner, C., Böttger, J., et al. (2013). Recent advances in 2D and 3D in vitro systems using primary hepatocytes, alternative hepatocyte sources and non-parenchymal liver cells and their use in investigating mechanisms of hepatotoxicity, cell signaling and ADME. Arch. Toxicol. *87*, 1315–1530.

Goldstein, I., and Hager, G.L. (2015). Transcriptional and chromatin regulation during fasting - The genomic era. Trends Endocrinol. Metab. *26*, 699–710.

Goldstein, I., Baek, S., Presman, D.M., Paakinaho, V., Swinstead, E.E., and Hager, G.L. (2017). Transcription factor assisted loading and enhancer dynamics dictate the hepatic fasting response. Genome Res *27*, 427–439.

Grimm, D., Kern, A., Rittner, K., and Kleinschmidt, J.A. (1998). Novel tools for production and purification of recombinant adenoassociated virus vectors. Hum. Gene Ther. *9*, 2745–2760.

He, B., Cruz-Topete, D., Oakley, R.H., Xiao, X., and Cidlowski, J.A. (2015). Human glucocorticoid receptor beta regulates gluconeogenesis and inflammation in mouse liver. Mol. Cell. Biol. *36*, 714–730.

Heinz, S., Benner, C., Spann, N., Bertolino, E., Lin, Y.C., Laslo, P., Cheng, J.X., Murre, C., Singh, H., and Glass, C.K. (2010). Simple combinations of lineage-determining transcription factors prime cis-regulatory elements required for macrophage and B cell identities. Mol. Cell *38*, 576–589.

Herzig, S., Long, F., Jhala, U.S., Hedrick, S., Quinn, R., Bauer, A., Rudolph, D., Schutz, G., Yoon, C., Puigserver, P., et al. (2001). CREB regulates hepatic gluconeogenesis through the coactivator PGC-1. Nature *413*, 179–183.

Huang, W., Metlakunta, A., Dedousis, N., Zhang, P., Sipula, I., Dube, J.J., Scott, D.K., and O'Doherty, R.M. (2010). Depletion of liver Kupffer cells prevents the development of diet-induced hepatic steatosis and insulin resistance. Diabetes *59*, 347–357.

John, S., Sabo, P.J., Thurman, R.E., Sung, M.H., Biddie, S.C., Johnson, T.A., Hager, G.L., and Stamatoyannopoulos, J.A. (2011). Chromatin accessibility pre-determines glucocorticoid receptor binding patterns. Nat. Genet. *43*, 264–268.

Jordan, S., Tung, N., Casanova-Acebes, M., Chang, C., Cantoni, C., Zhang, D., Wirtz, T.H., Naik, S., Rose, S.A., Brocker, C.N., et al. (2019). Dietary intake regulates the circulating inflammatory monocyte pool. Cell *178*, 1102–1114.e17.

Kanehisa, M., Sato, Y., Furumichi, M., Morishima, K., and Tanabe, M. (2019). New approach for understanding genome variations in KEGG. Nucleic Acids Res *47*, D590–D595.

Kersten, S., Seydoux, J., Peters, J.M., Gonzalez, F.J., Desvergne, B., and Wahli, W. (1999). Peroxisome proliferator-activated receptor alpha mediates the adaptive response to fasting. J. Clin. Invest. *103*, 1489–1498.

Kim, D., Paggi, J.M., Park, C., Bennett, C., and Salzberg, S.L. (2019). Graph-based genome alignment and genotyping with HISAT2 and HISAT-genotype. Nat. Biotechnol. *37*, 907–915.

Kleiman, A., Hübner, S., Rodriguez Parkitna, J.M., Neumann, A., Hofer, S., Weigand, M.A., Bauer, M., Schmid, W., Schütz, G., Libert, C., et al. (2012). Glucocorticoid receptor dimerization is required for survival in septic shock via suppression of interleukin-1 in macrophages. FASEB J *26*, 722–729.

Kulozik, P., Jones, A., Mattijssen, F., Rose, A.J., Reimann, A., Strzoda, D., Kleinsorg, S., Raupp, C., Kleinschmidt, J., Müller-Decker, K., et al. (2011). Hepatic deficiency in transcriptional cofactor TBL1 promotes liver steatosis and hypertriglyceridemia. Cell Metab *13*, 389–400.

Kumar, L., and Futschik, M.E. (2007). Mfuzz: a software package for soft clustering of microarray data. Bioinformation *2*, 5–7.

Lanthier, N., Molendi-Coste, O., Horsmans, Y., van Rooijen, N., Cani, P.D., and Leclercq, I.A. (2010). Kupffer cell activation is a causal factor for hepatic insulin resistance. Am. J. Physiol. Gastrointest. Liver Physiol. *298*, G107–G116.

Layer, R.M., Pedersen, B.S., DiSera, T., Marth, G.T., Gertz, J., and Quinlan, A.R. (2018). GIGGLE: a search engine for large-scale integrated genome analysis. Nat. Methods *15*, 123–126.

Li, H., and Durbin, R. (2009). Fast and accurate short read alignment with Burrows-Wheeler transform. Bioinformatics *25*, 1754–1760.

Li, H., Handsaker, B., Wysoker, A., Fennell, T., Ruan, J., Homer, N., Marth, G., Abecasis, G., and Durbin, R.; 1000 Genome Project Data Processing Subgroup (2009). The sequence alignment/map format and SAMtools. Bioinformatics *25*, 2078–2079.

Loft, A., Alfaro, A.J., Schmidt, S.F., Pedersen, F.B., Terkelsen, M.K., Puglia, M., Chow, K.K., Feuchtinger, A., Troullinaki, M., Maida, A., et al. (2021a). Liver-fibrosis-activated transcriptional networks govern hepatocyte reprogramming and intra-hepatic communication. Cell Metab *33*, 1685–1700.e9.

Loft, A., Herzig, S., and Schmidt, S.F. (2021b). Purification of GFP-tagged nuclei from frozen livers of INTACT mice for RNA- and ATAC-sequencing. Star Protoc *2*, 100805.

Love, M.I., Huber, W., and Anders, S. (2014). Moderated estimation of fold change and dispersion for RNA-seq data with DESeq2. Genome Biol *15*, 550.

Madsen, J.G., Schmidt, S.F., Larsen, B.D., Loft, A., Nielsen, R., and Mandrup, S. (2015). iRNA-seq: computational method for genome-wide assessment of acute transcriptional regulation from total RNA-seq data. Nucleic Acids Res *43*, e40.

Madsen, J.G.S., Rauch, A., Van Hauwaert, E.L., Schmidt, S.F., Winnefeld, M., and Mandrup, S. (2018). Integrated analysis of motif activity and gene expression changes of transcription factors. Genome Res *28*, 243–255.

Mo, A., Mukamel, E.A., Davis, F.P., Luo, C., Henry, G.L., Picard, S., Urich, M.A., Nery, J.R., Sejnowski, T.J., Lister, R., et al. (2015). Epigenomic signatures of neuronal diversity in the mammalian brain. Neuron *86*, 1369–1384.

Montagner, A., Polizzi, A., Fouché, E., Ducheix, S., Lippi, Y., Lasserre, F., Barquissau, V., Régnier, M., Lukowicz, C., Benhamed, F., et al. (2016). Liver PPARalpha is crucial for whole-body fatty acid homeostasis and is protective against NAFLD. Gut *65*, 1202–1214.

Mueller, K.M., Hartmann, K., Kaltenecker, D., Vettorazzi, S., Bauer, M., Mauser, L., Amann, S., Jall, S., Fischer, K., Esterbauer, H., et al. (2017). Adipocyte glucocorticoid receptor deficiency attenuates aging- and HFD-induced obesity and impairs the feeding-fasting transition. Diabetes *66*, 272–286.

Nathwani, A.C., Gray, J.T., Ng, C.Y., Zhou, J., Spence, Y., Waddington, S.N., Tuddenham, E.G., Kemball-Cook, G., McIntosh, J., Boon-Spijker, M., et al. (2006). Self-complementary adeno-associated virus vectors containing a novel liver-specific human factor IX expression cassette enable highly efficient transduction of murine and nonhuman primate liver. Blood *107*, 2653–2661.

Okawa, T., Nagai, M., and Hase, K. (2020). Dietary intervention impacts immune cell functions and dynamics by inducing metabolic rewiring. Front. Immunol. *11*, 623989.

Opherk, C., Tronche, F., Kellendonk, C., Kohlmüller, D., Schulze, A., Schmid, W., and Schütz, G. (2004). Inactivation of the glucocorticoid receptor in hepatocytes leads to fasting hypoglycemia and ameliorates hyperglycemia in streptozotocin-induced diabetes mellitus. Mol. Endocrinol. *18*, 1346–1353.

Pailla, K., Lim, S.K., De Bandt, J.P., Aussel, C., Giboudeau, J., Troupel, S., Cynober, L., and Blonde-Cynober, F. (1998). TNF-alpha and IL-6 synergistically inhibit ketogenesis from fatty acids and alpha-ketoisocaproate in isolated rat hepatocytes. JPEN J. Parenter. Enter. Nutr. *22*, 286–290.

Paumelle, R., Haas, J.T., Hennuyer, N., Baugé, E., Deleye, Y., Mesotten, D., Langouche, L., Vanhoutte, J., Cudejko, C., Wouters, K., et al. (2019). Hepatic PPARalpha is critical in the metabolic adaptation to sepsis. J. Hepatol. *70*, 963–973.

Peng, W.C., Logan, C.Y., Fish, M., Anbarchian, T., Aguisanda, F., Álvarez-Varela, A., Wu, P., Jin, Y., Zhu, J., Li, B., et al. (2018). Inflammatory cytokine TNFalpha promotes the long-term expansion of primary hepatocytes in 3D culture. Cell *175*, 1607–1619.e15.

Postic, C., Shiota, M., Niswender, K.D., Jetton, T.L., Chen, Y., Moates, J.M., Shelton, K.D., Lindner, J., Cherrington, A.D., and Magnuson, M.A. (1999). Dual roles for glucokinase in glucose homeostasis as determined by liver and pancreatic beta cell-specific gene knock-outs using Cre recombinase. J. Biol. Chem. *274*, 305–315.

Puchalska, P., Martin, S.E., Huang, X., Lengfeld, J.E., Daniel, B., Graham, M.J., Han, X., Nagy, L., Patti, G.J., and Crawford, P.A. (2019). Hepatocyte-macrophage acetoacetate shuttle protects against tissue fibrosis. Cell Metab *29*, 383–398.e7.

Qin, Q., Fan, J., Zheng, R., Wan, C., Mei, S., Wu, Q., Sun, H., Brown, M., Zhang, J., Meyer, C.A., et al. (2020). Lisa: Inferring transcriptional regulators through integrative modeling of public chromatin accessibility and ChIP-seq data. Genome Biol *21*, 32.

Ratman, D., Mylka, V., Bougarne, N., Pawlak, M., Caron, S., Hennuyer, N., Paumelle, R., De Cauwer, L., Thommis, J., Rider, M.H., et al. (2016). Chromatin recruitment of activated AMPK drives fasting response genes co-controlled by GR and PPARalpha. Nucleic Acids Res *44*, 10539–10553.

Rauch, A., Haakonsson, A.K., Madsen, J.G.S., Larsen, M., Forss, I., Madsen, M.R., Van Hauwaert, E.L., Wiwie, C., Jespersen, N.Z., Tencerova, M., et al. (2019). Osteogenesis depends on commissioning of a network of stem cell transcription factors that act as repressors of adipogenesis. Nat. Genet. *51*, 716–727.

Rose, A.J., Berriel Díaz, M., Reimann, A., Klement, J., Walcher, T., Krones-Herzig, A., Strobel, O., Werner, J., Peters, A., Kleyman, A., et al. (2011). Molecular control of systemic bile acid homeostasis by the liver glucocorticoid receptor. Cell Metab *14*, 123–130.

Sakai, M., Troutman, T.D., Seidman, J.S., Ouyang, Z., Spann, N.J., Abe, Y., Ego, K.M., Bruni, C.M., Deng, Z., Schlachetzki, J.C.M., et al. (2019). Liver-derived signals sequentially reprogram myeloid enhancers to initiate and maintain Kupffer cell identity. Immunity *51*, 655–670.e8.

Schmidt, S.F., Larsen, B.D., Loft, A., and Mandrup, S. (2016). Cofactor squelching: artifact or fact? BioEssays *38*, 618–626.

Schneider, C.A., Rasband, W.S., and Eliceiri, K.W. (2012). NIH Image to ImageJ: 25 years of image analysis. Nat. Methods *9*, 671–675.

Scott, C.L., Zheng, F., De Baetselier, P., Martens, L., Saeys, Y., De Prijck, S., Lippens, S., Abels, C., Schoonooghe, S., Raes, G., et al. (2016). Bone marrow-derived monocytes give rise to self-renewing and fully differentiated Kupffer cells. Nat. Commun. *7*, 10321.

Stienstra, R., Saudale, F., Duval, C., Keshtkar, S., Groener, J.E., van Rooijen, N., Staels, B., Kersten, S., and Müller, M. (2010). Kupffer cells promote hepatic steatosis via interleukin-1beta-dependent suppression of peroxisome proliferator-activated receptor alpha activity. Hepatology *51*, 511–522.

Van Wyngene, L., Vanderhaeghen, T., Timmermans, S., Vandewalle, J., Van Looveren, K., Souffriau, J., Wallaeys, C., Eggermont, M., Ernst, S., Van Hamme, E., et al. (2020). Hepatic PPARalpha function and lipid metabolic pathways are dysregulated in polymicrobial sepsis. EMBO Mol. Med. *12*, e11319.

Wang, A., Huen, S.C., Luan, H.H., Yu, S., Zhang, C., Gallezot, J.D., Booth, C.J., and Medzhitov, R. (2016). Opposing effects of fasting metabolism on tissue tolerance in bacterial and viral inflammation. Cell *166*, 1512–1525.e12.

Weis, S., Carlos, A.R., Moita, M.R., Singh, S., Blankenhaus, B., Cardoso, S., Larsen, R., Rebelo, S., Schäuble, S., Del Barrio, L., et al. (2017). Metabolic adaptation establishes disease tolerance to sepsis. Cell *169*, 1263–1275.e14.

Xiong, X., Kuang, H., Ansari, S., Liu, T., Gong, J., Wang, S., Zhao, X.Y., Ji, Y., Li, C., Guo, L., et al. (2019). Landscape of intercellular crosstalk in healthy and NASH liver revealed by single-cell secretome gene analysis. Mol. Cell *75*, 644–660.e5.

Young, M.D., Wakefield, M.J., Smyth, G.K., and Oshlack, A. (2010). Gene ontology analysis for RNA-seq: accounting for selection bias. Genome Biol *11*, R14.

STAR★METHODS

KEY RESOURCES TABLE

REAGENT or RESOURCE	SOURCE	IDENTIFIER
Antibodies		
Rabbit monoclonal anti-GFP antibody	Life Technologies	Cat: G10362; RRID: AB_2536526
Rabbit monoclonal anti-HNF-4-alpha antibody [EPR16885-99]	Abcam	Cat: ab231167; RRID: AB_2895610
Mouse monoclonal anti-HNF-4-alpha antibody [K9218]	Thermo Fisher Scientific	Cat: MA1−199; RRID: AB_2633309
Rabbit monoclonal anti-F4/80 [D2S9R]	Cell Signaling Technologies	Cat: 70076; RRID: AB_2799771
Rat monoclonal anti-F4/80 [CI:A3-1]	Abcam	Cat: ab6640; RRID: AB_1140040
Goat polyclonal anti-CLEC4F	R&D Systems	Cat: AF2784; RRID: AB_2081339
Rat monoclonal anti-Ki67	Synaptic Systems	Cat: HS−398117; RRID: AB_2744641
Rabbit monoclonal anti-Glucocorticoid Receptor [D6H2L]	Cell Signaling Technologies	Cat: 12041; RRID: AB_2631286
Rabbit polyclonal anti-Glucocorticoid Receptor	Proteintech	Cat: 24050–1-AP; RRID: AB_2813890
Mouse monoclonal anti-Glucocorticoid Receptor [BuGR2]	Thermo Fisher Scientific	Cat: MA1-510; RRID: AB_325427
Rabbit polyclonal anti-PPAR alpha	Abcam	Cat: ab24509; RRID: AB_448110
Rabbit polyclonal HSL antibody	Cell Signaling	Cat: 4107; RRID: AB_2296900
Rabbit polyclonal Phospho-HSL (Ser660) antibody	Cell Signaling	Cat: 45804; RRID: AB_2893315
Rabbit polyclonal Phospho-HSL (Ser565) antibody	Cell Signaling	Cat: 4137; RRID: AB_2135498
Rabbit Monoclonal Anti-TNF Antibody [EPR19147]	Abcam	Cat: ab183218; RRID: AB_2889388
Mouse monoclonal anti-β-Actin antibody [AC-15)	Sigma	Cat: A1978; RRID: AB_476692
Mouse monoclonal anti-Lamin A/C [4C11]	Cell Signaling Technologies	Cat: 4777; RRID: AB_10545756
Mouse monoclonal anti-α-Tubulin [TU-02]	Santa Cruz	Cat: sc-8035; RRID: AB_628408
Mouse monoclonal anti-VCP [clone 5]	Abcam	Cat: ab11433; RRID: AB_298039
Donkey anti-goat IgG, Alexa Fluor 555	Thermo Fisher Scientific	Cat: A−21432; RRID: AB_2535853
Donkey anti-mouse IgG, Alexa Fluor 555	Thermo Fisher Scientific	Cat: A−31570; RRID: AB_2536180
Goat anti-mouse IgG, Alexa Fluor 488	Thermo Fisher Scientific	Cat: A−11001; RRID: AB_2534069
Goat anti-rabbit IgG, Alexa Fluor 594	Thermo Fisher Scientific	Cat: A−11012; RRID: AB_2534079
Goat anti-rabbit IgG, Alexa Fluor 647	Thermo Fisher Scientific	Cat: A−21245; RRID: AB_2535813
Goat anti-rat IgG, Alexa Fluor 647	Thermo Fisher Scientific	Cat: A−21247; RRID: AB_141778
Rabbit anti-rat IgG, Biotinylated	Vector Laboratories	Cat: BA−4001; RRID: AB_10015300
Goat anti-rabbit IgG, Cyanine3	Thermo Fisher Scientific	Cat: A−10520; RRID: AB_2534029
Swine polyclonal anti-rabbit IgG, HRP	Agilent	Cat: P0399; RRID: AB_2617141
Goat polyclonal anti-mouse IgG, HRP	Agilent	Cat: P0447; RRID: AB_2617137
Bacterial and virus strains		
AAV-LP1-Cre	This study	N/A
AAV-LP1-Cremut	This study	N/A
Chemicals, peptides, and recombinant proteins		
Streptavidin linked CY5 (Zymax Grade)	Thermo Fisher Scientific	438316
Alexa-488-phalloidin	Thermo Fisher Scientific	A-12379
ProLong Gold antifade reagent	Thermo Fisher Scientific	P36934
Primary Hepatocyte Thawing and Plating Supplements	Thermo Fisher Scientific	CM3000
Primary Hepatocyte Maintenance Supplements	Thermo Fisher Scientific	CM4000
Corticosterone	Sigma	C2505
WY-14643	Sigma	C7081
Recombinant murine IL1β	Peprotech	211–11B
Recombinant murine TNF	Peprotech	315-01A
Lipopolysaccharide	Sigma	Cat: L2880; Batch: 05M4013V
Percoll	GE Healthcare	17089102

(*Continued on next page*)

Continued

REAGENT or RESOURCE	SOURCE	IDENTIFIER
Dexamethasone	Sigma	D4902
TRIzol	Life Technologies	15596018
EDTA-free Protease Inhibitor Cocktail	Roche	11873580001
RNasin Plus Rnase Inhibitor	Promega	N2615
Igepal CA-630	Sigma	56741
Protein G Dynabeads	Life Technologies	10004D
Amphotericin-B	Gibco	15290-026
DAPI	Sigma	D9542
Hoechst 33342	Thermo Fisher Scientific	62249
Critical commercial assays		
Insulin ELISA	Crystal Chem	90082
Corticosterone ELISA	Enzo	900-097
NEFA-HR(2) R1 and R2	Wako	434–91795; 436–91995
Serum Triglyceride Determination Kit	Sigma	TR0100
QuantiTect Reverse Transcription Kit	Qiagen	205311
VAHTS Stranded mRNA-seq Library Kit for Illumina	Vazyme	NR602
NEBNext Ultra RNA Library Prep Kit for Illumina	New England Biolabs	E7530L
TruePrep DNA Library Prep Kit V2 for Illumina	Vazyme	TD501
AMPure XP beads	Beckman	A63881
MinElute Reaction Cleanup kit	Qiagen	28204
Deposited data		
Microarray of livers from *Ppara*^{flox}; *Albumin-Cre*$^{+/-}$ and *Ppara*^{flox} mice, mice treated with vehicle or fenofibrate.	(Montagner et al., 2016)	GEO: GSE73298
Mircoarray of livers from *Nr3c1*^{flox}; *Albumin-Cre*$^{+/-}$ (GR^{HEP}) mice and *Nr3c1*^{flox} mice, mice treated with vehicle or dexamethasone.	(He et al., 2015)	GEO: GSE75682
RNA-seq of primary hepatocytes treated with vehicle, dexamethasone, GW7647 or a combination of dex/GW	(Ratman et al., 2016)	SRP058743
INTACT RNA-seq data	This study	GEO: GSE147923
INTACT ATAC-seq data	This study	GEO: GSE147922
Whole liver RNA-seq data	This study	GEO: GSE147924
Primary hepatocyte RNA-seq data	This study	GEO: GSE184765
Original code	This study	Zenodo Data: http://doi.org/10.5281/zenodo.5810134
Original western blot images	This study	Zenodo Data: http://doi.org/10.5281/zenodo.5810202
Experimental models: Cell lines		
HEPG2	ATCC	ATTC HB-8065
Experimental models: Organisms/strains		
B6;129-*Gt(ROSA)26Sor*$^{tm5(CAG-Sun1/sfGFP)Nat}$/J	JAX	Stock: 021039
B6N.Cg-*Speer6-ps1*$^{Tg(Alb-cre)21Mgn}$/J	JAX	Stock: 018961
B6N.129P2(B6)-*Lyz2*$^{tm1(cre)Ifo}$/J	JAX	Stock: 018956
Nr3c1^{tm2Gsc}*Lyz2*$^{tm1(cre)Ifo}$/J	(Kleiman et al., 2012)	N/A
C57BL/6J-*Clec4f*$^{em1(cre)Glass}$/J	JAX	Stock: 033296
Nr3c1^{tm2Gsc}*Clec4f*$^{em1(cre)Glass}$/J	This study	N/A
C57BL/6J (B6/J)	JAX	Stock: 000664
C57BL/6NCrl (B6/N)	Charles River	Strain code: 027

(*Continued on next page*)

Continued

REAGENT or RESOURCE	SOURCE	IDENTIFIER
Oligonucleotides		
Primers for detection of *Nr3c1*: *Nr3c1_f*: ggcatgcacattactggccttct	This study	N/A
Primers for detection of *Nr3c1*: *Nr3c1_r1*: gtgtagcagccagcttacagga	This study	N/A
Primers for detection of *Nr3c1*: *Nr3c1_r2*: ccttctcattccatgtcagcatgt	This study	N/A
qPCR primers	This study	Table S4
Recombinant DNA		
Plasmid: pdsAAV-LP1-Cre	This study	Zenodo Data: http://doi.org/10.5281/zenodo.5810475
Plasmid: pdsAAV-LP1-Cremut	This study	Zenodo Data: http://doi.org/10.5281/zenodo.5810475
Software and algorithms		
STAR	Dobin et al. (2013)	v2.4.2a / v2.6.1a
HISAT2	Kim et al. (2019)	v2.1.0
BWA aligner	Li and Durbin (2009)	v0.7.5a-r405
Samtools	Li et al. (2009)	v0.1.19-44428cd
iRNA-seq	Madsen et al. (2015)	v1.1
DESeq2	Love et al. (2014)	v1.24.0
HOMER	Heinz et al. (2010)	v4.10
IMAGE	Madsen et al. (2018)	v1.1
Mfuzz	Kumar and Futschik, 2007	v2.44.0
goseq	Young et al. (2010)	v1.36.0
KEGG PATHWAY database collection	Kanehisa et al. (2019)	https://www.genome.jp/kegg/
Lisa	Qin et al. (2020)	http://lisa.cistrome.org/
NicheNet	Browaeys et al. (2020)	v0.1.0
CistromeDB toolkit / GIGGLE	Layer et al. (2018)	http://dbtoolkit.cistrome.org/
ImageJ	Schneider et al. (2012)	https://imagej.net/software/fiji/
Other		
Rodent Chow Pellets	Altromin	1314
RPMI-1640	Sigma	R8758
William's E Medium	Sigma	W1878
DMEM, low glucose	Gibco	11885084
DMEM, no glucose, no glutamine, no phenol red	Gibco	A1443001
FBS	Sigma	F7524
FBS	Gibco	10270
Corning BioCoat Collagen I cell culture plates	VWR	734-0166
EconoSpin Micro/Mini Columns	Epoch	3010-250/1920-250

RESOURCE AVAILABILITY

Lead contact

Further information and requests for resources and reagents should be directed to and will be fulfilled by the Lead Contact, Stephan Herzig (Stephan.herzig@helmholtz-muenchen.de).

Materials availability

New reagents and materials generated in this study are listed in the key resources table and will be made available on request, but we may require a completed Materials Transfer Agreement if there is potential for commercial application.

Data and code availability

- RNA-seq and ATAC-seq data have been deposited at GEO and are publicly available as of the date of publication. Accession numbers are listed in the key resources table. Original western blot images have been deposited at Zenodo and are publicly available as of the date of publication. The DOI is listed in the key resources table. Microscopy data reported in this paper will be shared by the lead contact upon request.
- All original code has been deposited at Zenodo and is publicly available as of the date of publication. The DOI is listed in the key resources table.
- Any additional information required to reanalyze the data reported in this paper is available from the lead contact upon request.

EXPERIMENTAL MODEL AND SUBJECT DETAILS

Animal models and experiments

All animal studies were conducted in accordance with German animal welfare legislation and protocols were approved by the state ethics committees and government of Upper, Bavaria (License # 55.2-1-55-2532-49-2017 and 55.2-1-54-2532.0-40-15) and the Regierungspräsidium Tübingen (License #1332 and #1512). All mice were maintained in a climate-controlled environment at ~23°C and constant humidity with specific pathogen-free conditions under strict 12 h dark-light cycles (6:00 a.m. to 6:00 p.m.). All mice had *ad libitum* access to food and water and before the start of experiments, all mice were maintained on a regular chow diet (Altromin, 1314). For fasting studies, food was removed 30 min before lights off for the indicated duration of time.

B6;129 *Gt(ROSA)26Sor*$^{tm5(CAG-Sun1/sfGFP)Nat}$/J mice (Mo et al., 2015) used in this study were backcrossed to C57BL/6NCrl (B6/N) (Charles Rivers) using a speed congenics approach to ensure a > 95 % genetic B6/N background. These were then crossed with B6N.Cg-*Speer6-ps1*$^{Tg(Alb-cre)21Mgn}$/J (Alb-Cre) (Postic et al., 1999) or B6N.129P2(B6)-*Lyz2*$^{tm1(cre)Ifo}$/J (LysMCre) (Clausen et al., 1999) mice to generate HEP-INTACT and MAC-INTACT mice with hepatocyte-specific and myeloid-specific GFP tagging of the nuclear membrane. Mice referred to as GR^{MAC} mice were generated from GR^{flox} (*Nr3c1*^{tmGsc}) crossed to LysMCre mice (*Nr3c1*^{tmGsc}*Lyz2*$^{tm19(cre)ifo}$/J) and maintained on a C57BL/6J (B6/J) background, as previously described (Kleiman et al., 2012). GR^{KC} mice were generated from GR^{flox} (*Nr3c1*^{tmGsc}) crossed to C57BL/6J-*Clec4f*$^{em1(cre)Glass}$/J mice (Sakai et al., 2019) purchased from JAX, and maintained on a B6/J background. To confirm a specific deletion of GR in liver macrophages, DNA was isolated from indicated organs and tissues of the GR^{KC} mice and the PCR reaction was set up using One*Taq* Hot Start DNA polymerase (NEB) and primers to detect bands corresponding to the floxed and deleted *Nr3c1*. Resulting PCR products were run on a 1.5% agarose gel.

For sepsis experiments, 10–12-weeks-old male GR^{flox} or GR^{MAC} littermates were injected intraperitoneally with 10 mg/kg lipopolysaccharide (LPS) (Sigma) or saline vehicle. Mice were weighed and core temperature determined by rectal probe every 4 h.

For double knockout experiments, 8–10-weeks-old female and male GR^{flox} or GR^{MAC} littermates were injected intravenously with adenovirus associated virus encoding the Cre recombinase (AAV-Cre) or a mutated form of Cre (AAV-Cre^{mut}). 4 weeks post injection mice were fasted for 8 h, as indicated. At least once per week the health status of mice was monitored and weight was recorded, and all mice used for experiments displayed good general health. During the mouse experiments, animal caretakers and investigators conducting the experiments were generally not blinded to the group allocation of mice. The total number of mice analyzed for each experiment is detailed in the figure legends.

Isolation and culture of primary cells and cell lines

Mouse primary hepatocytes were isolated from 8-12 weeks old B6/N mice and liver macrophages were isolated from 8-12 weeks old B6/J, GR^{flox} and GR^{MAC} mice by perfusing the liver of mice with 15 mL of pre-perfusion buffer (Hanks' balanced salt solution (HBSS) (Sigma), 10 mM HEPES, 0.5 mM EDTA)), followed by 15 mL of collagenase digestion buffer (HBSS, 5 mM $CaCl_2$, 1 mM HEPES, 0.4 mg/mL collagenase (Sigma #C5138) using a peristaltic pump (VWR). Liver cells were released and passed through a 70-μm cell strainer (Greiner) and centrifuged at 50g for 1 min at 4 °C to pellet the parenchymal cells, which subsequently were washed twice, resuspended and stored in suspension buffer as described in Godoy et al. (2013). To pellet the non-parenchymal cells, the supernatant was then centrifuged at 300g for 5 min at 4 °C. The pellet was resuspended in erylysis buffer and incubated for 15 min at 4°C before centrifugation at 300g for 5 min at 4 °C . Resulting pellet was resuspended in 25 % Percoll (GE Healthcare) in DMEM (Sigma) and centrifuged at 300g for 10 min at 4°C . Resulting pellet was resuspended in RPMI-1640 medium (Sigma) supplemented with 10 % fetal bovine serum (FBS) (Sigma), 1% penicillin-streptomycin (Sigma) and 1% amphotericin-B (Gibco) and cultured at 37°C and 5% CO_2 for up to 3 d. Liver macrophages isolated from GR^{flox} and GR^{MAC} were treated with either vehicle (DMSO) or Dex (100 nM) (Sigma) for 8 h, then washed 3× with PBS to remove all residual Dex. Medium was replaced with RPMI-1640 containing 10 % FBS and conditioned for 24 h. HEPG2 cells (passage < 12) were cultured in DMEM (Gibco) containing 10 % FBS and 1 % PS and subsequently treated with liver-macrophage-conditioned medium, diluted 1:1 with serum free DMEM (Sigma).

For primary hepatocyte culture experiments, 400.000 cells per well were plated in collagen-coated 12-well plates (Corning) in plating medium (William's Medium E (WME) (Sigma) containing 5 % FBS (Gibco), 1× Thawing and Plating Supplements (minus Dex) (Thermo Fisher Scientific) and 1 μM corticosterone (Cort) (Sigma)) and maintained at 37 °C and 5 % CO_2. After 1 h, cells were washed with PBS (Thermo Fisher Scientific) and medium was changed to maintenance medium (WME, containing 1× Maintenance Supplements (minus Dex) (Thermo Fisher Scientific) and 0.1 μM Cort). After 6 h, medium was changed to starvation medium (DMEM without glucose (Gibco), 1 % P/S, 1 % FBS, and 5-mM glucose) and incubated 16 h. Cells were then treated for 8 h with 1 μM

Cort and 10 μM WY-14643 (WY) (Sigma) alone or in combination, and co-treated with 0.2, 1, or 5 ng/mL TNF (PeproTech) or 1 ng/mL IL1β (PeproTech) as indicated. For conditioned media experiments, primary hepatocytes were treated with liver-macrophage-conditioned medium supplemented with 1 μM Cort and 10 μM WY for 8 h.

METHOD DETAILS

Adeno-associated virus (AAV) generation

pdsAAV-LP1-Cre was generated by insertion of the Cre transgene into pdsAAV-LP1-GFPmut-miR-NC (Rose et al., 2011) thereby removing the regions harboring GFPmut and miR-NC.pdsAAV-LP1-Cremut was generated through disruption of the start codon of Cre and generation of 2 stop codons proximal to the translational starting point. AAV packaging and titer determination by qPCR against viral genomes was performed by Vigene, using the pDGΔVP helper plasmid (Grimm et al., 1998) and a mutated p5E18-VD2/8 expression vector (Gao et al., 2002) encoding AAV2 rep and a mutated AAV8 cap protein (aa 589–592: QNTA to GNRQ).

Isolation of GFP-tagged nuclei

Liver tissue from INTACT mice was rapidly dissected in PBS and snap-frozen in liquid nitrogen and GFP+ hepatocyte- and liver macrophage-nuclei were enriched using the INTACT liver protocol (Loft et al., 2021a, 2021b). In brief, liver tissue was crushed into fine powder using a Tissuelyzer II (Qiagen) and subsequently washed in PBS. The tissue was Dounce homogenized using 10× loose pestle in 5 mL of low sucrose buffer (LSB: 0.25 M sucrose, 25 mM KCl, 5 mM $MgCl_2$, 20 mM Tris-HCl (pH 7.5), 1 mM 1,4-dithiothreitol (DTT), 0.15 mM spermine, 0.5 mM spermidine, 1× EDTA-free protease inhibitor cocktail (PIC) (Roche), and 60 U/mL RNasin Plus Rnase Inhibitor (Promega)) per 0.5 mg of tissue, then added 0.35 % Igepal CA-630 (Sigma) and left on ice for 5 min followed by further douncing 5× with the tight pestle. The homogenate was filtered through a 100μm CellTrics filter unit (Sysmex Deutschland) and spun down 600g for 10 min at 4 °C. The pellet was resuspended in 9× high sucrose buffer (same as LSB, but with 2 M sucrose) and centrifuged 15,000g for 15 min at 4 °C. The nuclei pellet was subsequently resuspended in wash buffer (LSB with 0.35 % Igepal CA-630) and an aliquot of whole liver nuclei was kept on ice for later analyses. Pre-clearing of nuclei (15 mill nuclei per HEP-INTACT mouse and 80 mill nuclei per MAC-INTACT mouse) was done by incubating with 20 μL of Protein G Dynabeads (Life Technologies) for 15 min. After removal of the beads on a magnet, the solution was incubated with 3 μg rabbit monoclonal anti-GFP antibody (Life Technologies) for 30 min. Then 80 μL of Dynabeads was added and the solution was incubated for additional 20 min. Bead-bound nuclei were washed 3× in 2 mL wash buffer (without RNasin) using a magnet. All steps were performed on ice or in the cold room, and all incubations were carried out using an end-to-end rotator.

Serum, plasma and liver assays

Blood glucose and β-hydroxybutyrate in mice were measured directly via blood from the tail tips using a GK dual glucose and ketone meter (Swiss Point of Care). Measurements of serum insulin (Crystal Chem) and corticosterone (Enzo) in mice were performed using enzyme immunoassay kits and serum NEFA was measured using a colorimetric assay (Wako). For measurements of liver TG levels, 50 mg liver was homogenized in isopropanol and supernatant was collected for enzymatic colorimetric measurements (Sigma).

Histology and image analyses

Dissected liver samples from 8–12-weeks-old HEP-INTACT, GR^{flox} and GR^{MAC} mice were flash frozen in liquid nitrogen and cryosectioned at 12 μm. Immunohistochemical staining on sections from HEP-INTACT mice was performed using rabbit anti-HNF4α (1:2000; Abcam) and Cyanine3-conjugated anti-rabbit (1:100; Thermo Fisher Scientific), and co-staining was performed on sections from GR^{flox} and GR^{MAC} mice using anti-GR (1:200; Proteintech), anti-HNF4α (1:100; Thermo Fisher Scientific), anti-rabbit Alexa Fluor-647 (1:300; Thermo Fisher Scientific) and anti-mouse Alexa Fluor-488 (1:300; Thermo Fisher Scientific). Liver tissue specimen from 8–12-weeks-old B6/N and MAC-INTACT mice were fixed in 4 % (w/v) neutrally buffered formaldehyde solution and subsequently routinely embedded in paraffin. 3 μm thick sections from B6/N mice were co-stained using anti-CLEC4F (1:50; R and D Systems), anti-KI67 (1:100; Synaptic Systems), anti-goat Alexa Fluor-555 (1:100; Thermo Fisher Scientific), anti-rat biotin-linked IgG (1:300; Vector Laboratories) and streptavidin-linked Cyanine5 (1:100; Thermo Fisher Scientific). 5 μm thick sections from MAC-INTACT mice were co-stained using anti-F4/80 (1:200; Abcam), anti GFP-tag (1:75; Thermo Fisher Scientific), anti-rat Alexa Fluor-647 (1:400; Thermo Fisher Scientific) and anti-rabbit Cyanine3 (1:100; Thermo Fisher Scientific). After washing, nuclei were stained with Hoechst-33342 or DAPI and mounted using ProLong Gold antifade reagent (Thermo Fisher Scientific). Fluorescence stainings from INTACT mouse livers were photographed with an Axio Imager Z1 (Zeiss) and visualized with the Axio Vision 4.6.3 software (Zeiss). Stained slides from B6/N mouse livers were digitally scanned with an Axio Scan.Z1 scanner (Zeiss, Germany), using a 20× objective. Morphometric evaluation of the stained sections was performed using the commercially available software Definiens Developer XD 2 (Definiens AG). For INTACT mice, the calculated parameters were the percentage of GFP+ nuclei and double GFP+/HNF4α+ or GFP+/F4/80+ based on total number of nuclei. For B6/N mice, we calculated the percentage of double CLEC4F+/KI67+ nuclei of total CLEC4F+ nuclei as well as the CLEC4F+ area per total sectioned liver area. Stainings from GR^{flox} and GR^{MAC} mice liver were photographed with a Leica TCS SP8 microscope (Leica) and analyzed with ImageJ (Schneider et al., 2012). GR nuclear fluorescence intensity was determined by analyzing the GR signal in double DAPI+/HNF4α+ hepatocyte nuclei using an average of all hepatocytes in 3 fields per mouse.

For immunohistochemical analyses of primary hepatocytes and liver macrophages, these were fixed in 4% PFA for 15 min at 4 °C, washed 2x with PBS then permeabilized with 0.1 % TritonX-100 (Sigma) in PBS for 10-30 min at 4 °C. Liver macrophages were blocked overnight in blocking buffer (0.1 % TritonX-100, 1 % FBS (Sigma) in PBS) at 4 °C. After washing, cells were incubated with anti-F4/80 (1:200 in blocking buffer; Cell Signaling Technologies) and incubated overnight at 4 °C. Cells were washed with PBS, then incubated for 2 h at RT with anti-rabbit Alexa Fluor-594 (1:300; Thermo Fisher Scientific). Cells were again washed and stained with DAPI. Fluorescence was imaged using a Leica DWI 6000 B microscope with a Leica DFC 365 FX camera at 10× original magnification and the percentage of F4/80+ cells was determined using ImageJ. Primary hepatocyte cultures were blocked in 10 % horse serum for 10 min at RT and subsequently treated with anti-GR (1:100 in 5 % horse serum; Thermo Fisher Scientific) for 1 h. Cells were washed 3x in PBS and incubated for 1 h with anti-mouse Alexa Fluor-555 (1:1000; Thermo Fisher Scientific) and Alexa-488-phalloidin (1:200; Thermo Fisher Scientific). Subsequently cells were washed 2x with PBS and stained with DAPI, then mounted onto glass slides with 0.1 g/mL Mowiol. Immunofluorescent samples were analyzed using a Laser Scanning Confocal Microscope (Olympus Fluoview 1200, Olympus) equipped with an Olympus UPlanSApo 60x 1.35 and an UPlanSApo 40x 1.25Sil Oil immersion objective (Olympus). Quantification of the mean fluorescence per nuclei was performed in individual images after background subtraction with a minimum of 30 cells from three biological replicates using ImageJ.

Protein analysis

Frozen liver tissue was homogenized directly in cell lysis buffer (1 % Igepal, 150 mM NaCl, 50 mM Tris-Hcl (pH 6.8), 1 mM EDTA, 0.5 mM DTT) using the Tissuelyzer II. For nuclear protein extraction, 50-100 mg of liver tissue was Dounce homogenized using 10x loose and 10x tight pestle in 1 mL nuclei preparation buffer (0.25 M sucrose, 10 mM KCl, 1.5 mM $MgCl_2$, 10 mM Tris-HCL (pH 7.5), 0.2 mM DTT, 0.5 mM spermidine, 1x EDTA-free protease inhibitor, and 1x PhosSTOP). The homogenate was filtered through a 70 μm CellTrics filter unit and isolated nuclei was obtained by washing and spinning 3x 500g for 10 min at 4 °C. Isolated nuclei was resupended in RIPA buffer (50 mM Tris-HCl (pH 8.0), 150 mM NaCl, 1 mM EDTA, 0.5 mM EGTA, 1 % Igepal CA-630, 0.1 % SDS, 0.5 % sodium deoxycholate (Sigma) supplemented with 1x PIC and 1xPhosSTOP). Adipose tissue was homogenized in RIPA buffer using the Precellys 24 (Peqlab). For immunoblot analysis, 20–30 μg of whole liver lysates, 7.5 μg of nuclear extracts or 20 μg of adipose tissue lysates were run on an SDS–PAGE gels (Novex WedgeWell, Tris-Glycine Mini Gels; Thermo Fisher Scientific, or Mini-PROTEAN Precast Gels; Bio-Rad Laboratories), transferred to 0.45 μM polyvinylidene difluoride membranes and incubated with primary antibodies against GR (1:1000; 12041; Cell Signaling), PPARα (1:2000; ab24509; Abcam), TNF (1:2000; ab183218; Abcam), Lamin A/C (1:4000; 4777; Cell Signaling), VCP (1:10000; ab11433; Abcam), HSL (1:1000; 4107; Cell Signaling), Phospho-HSL (Ser660) (1:1000; 45804; Cell Signaling), Phospho-HSL (Ser565) (1:1000; 4137; Cell Signaling), β-actin (1:2000; A1978; Sigma) and α-Tubulin (1:1,000; sc-8035; Santa Cruz). The following HRP-tagged secondary antibodies were used: Swine Anti-Rabbit Immunoglobulins (1:10000; P039901-2; Dako/Agilent) and Goat Anti-Mouse Immunoglobulins (1:10000; P044701-2; Dako/Agilent). Protein bands were detected with Immobilon Classico Western HRP substrate (Merck Millipore) or SuperSignal West Femto Maximum Sensitivity Substrate (Thermo Fisher Scientific) using an Amersham Imager 680 (GE Healthcare) or ChemiDoc MP Imager (Bio-Rad) and quantified with ImageJ.

RNA isolation and quantitative PCR analysis

Cultured liver macrophages and hepatocytes were washed once with cold PBS and lyzed using TRIzol (Life Technologies). Liver tissue was homogenized directly in TRIzol using a Tissuelyzer II (Qiagen). Whole liver nuclei as well as bead-bound and supernatant nuclei prepared from INTACT mice were directly resuspended in TRIzol. RNA purification was performed using EconoSpin columns (Epoch) with on-column DNase digestion (Qiagen). cDNA was transcribed using the QuantiTect Reverse Transcription Kit (Qiagen). RT–PCR was conducted using SYBR Green PCR Master Mix (Life technologies, Darmstadt, Germany) and the reaction was performed using the QuantStudio6 system (Life technologies, Darmstadt, Germany). All values were initially normalized to the reference gene *Tbp*, and subsequently all values within an experiment were adjusted to set the mean of the control condition to 1. Primary hepatocyte experiments were corrected for batch effects on overall expression levels, by dividing all values obtained from one mouse with the average across all the conditions from that mouse. For estimation of GR dependency, 14 genes were initially confirmed as PPARα target genes (significantly induced between the cort and cort+wy conditions), and their GR dependency index (GR_{DI}) was calculated using the formula: $GR_{DI} = log2\frac{WY+Cort}{WY} - log2\frac{WY}{Ctrl}$

RNA-seq library construction and sequencing

For RNA-seq of nuclei from INTACT mice, total RNA (50–100 ng) was prepared for sequencing using VAHTS Stranded mRNA-seq Library Kit for Illumina (Vazyme) following manufacturer's recommendations, except that no selection for poly-adenylated RNA was performed. For RNA-seq of whole liver, library preparation and sequencing were performed in house or by Novogene. In brief, a total amount of 500–1000 ng of total RNA was used and sequencing libraries were generated using NEBNext Ultra RNA Library Prep Kit for Illumina (NEB) following manufacturer's recommendations. Prepared PCR products were purified and size-selected on AMPure XP beads (Beckman), and library quality was assessed on the Agilent Bioanalyzer 2100 system. The prepared libraries were sequenced (paired-end) on an Illumina platform.

ATAC-seq library construction and sequencing

Approximately 25,000 bead-bound nuclei from INTACT animals were transposed in a 50 μL volume of 1X TTBL buffer and 3.5 μL TTE Mix V50 (from TruePrep DNA Library Prep Kit V2 for Illumina, Vazyme) for 30 minutes at 37°C. ATAC-seq reactions on GFP+ nuclei

obtained from livers of MAC-INTACT mice were made in technical duplicates. Fragmented genomic DNA was recovered using Buffer ERC coupled with MinElute spin column purification (Qiagen). Transposed genomic DNA was amplified by 12–14 cycles of quantitative PCR. Amplified DNA was purified and size-selected on AMPure XP beads (Beckman), analyzed on an Agilent Bioanalyzer, and sequenced (paired-end) on an Illumina HiSeq 4000 platform.

Processing and analyses of INTACT RNA-seq data

For INTACT RNA-seq libraries, the STAR aligner (v2.4.2a) (Dobin et al., 2013) with modified parameter settings (–twopassMode=Basic) was used for split-read alignment against the mouse genome assembly mm10 and UCSC knownGene annotation. Quantification of the number of mapped reads of each gene was performed using iRNA-seq (v1.1) (Madsen et al., 2015) specifying the "-count gene" option. For INTACT RNA-seq data obtained in hepatocytes and macrophages, we collected a set of cell type-selective genes regulated at one or more time points during fasting using DESeq2 (v1.24.0) (Love et al., 2014) specifying ''independentFiltering'' to be FALSE. This was accomplished by first determining differential expression (padj < 0.05) at the individual time points between the fed and the fasted conditions in hepatocytes and macrophages, respectively. Further, to define genes that were selectively expressed in macrophages in the liver, all IP fed or fasted conditions were tested against all input fed or fasted conditions. The set of macrophage genes were then identified as genes expressed in a macrophage-selective manner in both the fed and fasted conditions (padj < 0.05). A set of macrophage-expressed genes not regulated at any time point during fasting (padj > 0.05) were also defined. Hepatocyte-selective genes (padj < 0.05) were determined using a similar strategy by comparing the gene expression between hepatocytes and macrophages. Additionally, input-selective genes (padj < 0.05) were filtered out from the list of hepatocyte-selective genes. The resulting list of cell type-selective, fasting-regulated genes was subjected to soft clustering using Mfuzz (v2.44.0) (Kumar and Futschik, 2007) based on the log2FC in gene expression between fed and fasted condition at each individual time point. For this purpose, we defined the expression change at fasting start point as ''zero'' and standardized the expression changes at all other time points using ''standardise2'' (i.e., so that the expression change at fasting start point was regarded as zero and the standard deviation of the expression changes of individual genes was set at 1). Furthermore, we calculated the minimum centroid distance for a range of cluster numbers as a reference to choose an optimized number of clusters and only included genes with a membership value higher than 0.5 for further analyses. Functional enrichment analyses of genes within each cluster were performed with 'goseq' (v1.36.0) (Young et al., 2010) using the KEGG PATHWAY database collection (Kanehisa et al., 2019), excluding generic terms with more than 1,000 genes as well as disease terms (i.e. 05XXX).

NicheNet ligand activity and secretome analyses

To perform ligand activity analysis, we first defined the set of potentially active ligands in the ''sender'' cell population. Database information on ligand-receptor interactions were downloaded from https://zenodo.org/record/3260758/files/lr_network.rds and all fasting-regulated ligands for which at least one specific receptor was expressed (average mean expression over all conditions > 1 tag / kilobase (kb)) in the receiver cell population (i.e., hepatocytes or macrophages) was considered for further analyses. We then used NicheNet (v0.1.0) (Browaeys et al., 2020) to rank the ligands based on how well they predicted if a gene belongs to a gene set of interest compared to the background gene set. The gene sets of interest for macrophages and hepatocytes were defined as the fasting-regulated, KEGG-annotated genes belonging to the cluster in which the indicated KEGG pathway was enriched. As background, we used all other genes expressed in the receiver population (average mean expression over all conditions > 1 tag / kb). Ligand activity scores were calculated as the Pearson correlation coefficient between the ligand-target regulatory potential scores of each selected ligand and the target indicator vector, which indicates whether a gene belongs to the gene set of interest or not. For the top 5 ligands with highest ligand activity, the corresponding receptors were depicted in a ligand-receptor heatmap, where the ligand-receptor potential score accords to the weight of the interaction between the ligand and receptor in the weighted ligand signaling network downloaded from https://zenodo.org/record/3260758/files/weighted_networks.rds. Furthermore, the most prominent target genes for the top 5 ligands were selected based on the regulatory potential score, where genes depicted belonged to the indicated gene set of interested and were among the 2,500 most strongly predicted targets of at least one of the top 5 ligands. Ligand-target gene interactions was displayed in a circle plot using the R-package 'circlize' (v0.4.9).

Since NicheNet infers ligand activities based on a priori knowledge models on ligand-receptor-target interactions, we also undertook a more unbiased approach to identify novel putative, regulatory macrophage-derived secreted factors in fasting. Here, we obtained a comprehensive mouse secretome database from Xiong et al. (2019), which was intersected with the gene list containing macrophage-selective genes regulated at early time points (i.e., 3h and/or 8h) during fasting. We also used this gene list to explore how macrophage secretome genes were affected by loss of GR in macrophages. In this case, the *Lyz2* gene was removed from the gene list, since Cre is inserted into this gene in GR^{MAC} mice.

The NicheNet analyses on GR^{MAC} mice were performed using essentially the same strategy, as described above, except that the set of potentially active ligands were defined from macrophage-specific secretome genes confirmed to be regulated by macrophage GR by qPCR. Furthermore, the gene set of interest was defined as hepatocyte-specific, GR^{MAC}-repressed genes, which were among the most highly induced (padj < 0.00001) in hepatocytes after 3 and 8 h of fasting. For visualization purposes, the regulatory potential score was set to 0 if the score was among the 10 % lowest interaction scores between the top 5 ligands and their respective top targets.

Processing and analyses of bulk RNA-seq data

For whole liver RNA-seq libraries, paired-end reads were mapped to the mouse genome assembly mm10 using HISAT2 software (v2.1.0) (Kim et al., 2019) or the STAR aligner (Dobin et al., 2013). Quantification of the number of mapped reads of each gene were performed using iRNA-seq (v1.1) (Madsen et al., 2015) specifying the "-count gene" option. iRNA-seq was also used to call differentially expressed genes using standard parameters for the primary hepatocyte RNA-seq data. We called differentially expressed genes in GR^{MAC} vs GR^{flox} mice using DESeq2 (padj < 0.05) with default settings. These lists of regulated genes were intersected with the lists of hepatocyte and macrophage-selective genes identified from the INTACT RNA-seq analyses, and functional enrichment analyses of the different gene groups were performed using 'goseq' (v1.36.0) (Young et al., 2010), as described above.

Epigenetic landscape *in silico* deletion analysis

To predict TFs and chromatin regulators responsible for the regulation of GR^{MAC}-regulated gene programs, we performed epigenetic Landscape In Silico deletion Analysis (Lisa) (Qin et al., 2020) using the online application (http://lisa.cistrome.org/). In brief, Lisa computes a TF ranking table by combining the cistrome regulatory potential (Peak-RP) method, and H3K27ac/DNase-seq in silico deletion of TF ChIP-seq peaks. From this table, we selected the top predicted regulatory TFs for both hepatocyte-selective and macrophage-selective genes based on the most significant median p-values obtained from 4 different ChIP-seq profiles for each TF. For these top predicted TFs, we further inspected the related p-values from the TF ranking based solely on chromatin profile knockout of motif hit site, i.e., independent of ChIP-seq data.

Processing and analyses of ATAC-seq data

Sequence tags from ATAC-seq libraries were aligned to the mm10 using the BWA aligner (v0.7.5a-r405) (Li and Durbin, 2009). Post-alignment processing of reads was performed with Samtools (v0.1.19-44428cd) (Li et al., 2009) by removing duplicate reads and filtering for high quality reads using Samtools view using the following settings "-b -h -f 1 -F 4 -F 8 -F 256 -F 2048 -q 30". Furthermore, we only used reads with a fragment length < 100bp, corresponding to the reads located in nucleosome-free regions. ATAC seq peaks were identified, annotated and tags in peaks were counted using HOMER (v4.10) (Heinz et al., 2010). Tag directories from conditions with technical duplicates were combined into one before further analyses. For visualization purposes, the individual tag directories of one condition were merged into one and bedgraphs were generated using HOMER makeUCSCfile specifying '-fragLength 70' and '-fsize 20e'. For identification of accessible chromatin regions, peaks were called in each library with HOMER findPeaks using the following settings: 'peaks', '-fragLength 70', '-style factor', '-minDist 140', '-size 70'. For all peak files, overlapping peaks were merged and collected in one master peak file. Tags were then counted in a 200 bp window around the peak centers for each individual library in the resulting master peak file. From this peak file mitochondrial peaks were removed, and high confident peaks were identified as having at least 20 tags per 200 bp window in all 4 replicates for one or more of the conditions. Peaks with different tag count between hepatocytes and macrophages were identified using DESeq2 and macrophage-selective peaks were removed from the hepatocyte peak file and vice versa before subsequent analyses (padj < 0.1). For both cell types, we identified dynamic enhancers as ATAC-seq peaks regulated at one or more time points during fasting in the particular cell type (padj < 0.05). The resulting list of dynamic enhancers was subjected to soft clustering using Mfuzz (v2.44.0) (Kumar and Futschik, 2007) using a similar strategy as described above for gene expression clustering (i.e., clustering was done based on the log2FC in ATAC-seq tag count between fed and fasted condition at each individual time point, only including sites with a membership value higher than 0.5).

TF motif activity, target sites and genes

To compute the relative contribution of TF motifs to enhancer activity and gene expression in a given condition, we used IMAGE (v1.1) that applies a motif response analyses approach to integrate enhancer (ATAC-seq) and gene expression (RNA-seq) activities. We calculated the activity of a particular motif for a given sample by estimating the average contribution of that motif to the activity of all identified enhancers. Dynamic motifs were defined as motif activities changed at one or more time points during fasting in the particular cell type, which was calculated using an unpaired two-tailed Student's t test corrected by the Benjamini & Hochberg method (padj < 0.05). The resulting list of dynamic motif activities was subjected to soft clustering using Mfuzz (v2.44.0) (Kumar and Futschik, 2007) using a similar strategy as described above for gene expression clustering (i.e., clustering was done based on the delta value in motif activity between fed and fasted condition at each individual time point, only including motifs with a membership value > 0.35). We also used IMAGE to predict target sites and target genes (TGs) for all motifs and used this information to predict key regulators of each RNA-seq cluster from the list of IMAGE-predicted causal TFs. This was done by asking if the individual RNA-seq clusters were enriched for IMAGE-predicted TGs of each individual TF assigned to a motif activity cluster over a random distribution, essentially as previously described (Rauch et al., 2019): $Enrichment_{TG} = log_2 \frac{\frac{TG \in RNAseqCl}{TG+RNAseqCl}}{allExprGenes}$. For each RNA-seq cluster we selected the top 5 IMAGE-predicted causal (confidence 1 or 2) TFs with highest TG enrichment and at least 2-fold over random and depicted the enrichment of these TFs for all RNA-seq clusters in a heatmap. Furthermore, we validated the predicted GR target sites by calculating the similarity between the IMAGE-predicted GR target sites and the comprehensive collection of TF/chromatin regulator bulk sequencing data from the Cistrome Data Browser (CistromeDB) using the Giggle score (Layer et al., 2018) via the CistromeDB toolkit (http://dbtoolkit.cistrome.org/).

Analyses of public datasets

We used GEO2R to analyze microarray data obtained from livers of *Ppara*^{flox}*; Albumin-Cre*$^{+/-}$ (PPARα^{HEP}) mice and PPARα^{flox} mice treated with vehicle or fenofibrate for 10 d (GEO: GSE73298) (Montagner et al., 2016) as well as GR^{HEP} and GR^{flox} mice treated with vehicle or dex for 6 h (GEO: GSE75682) (He et al., 2015). From these datasets, we defined PPARα target genes as either being downregulated in PPARα^{HEP} versus PPARα^{flox} mice and GR target genes as being downregulated in GR^{HEP} versus GR^{flox} mice (padj < 0.05), as well as dual PPARα/GR hepatocyte targets genes being regulated in both conditions. By analyzing the microarray data from GR^{flox} and GR^{HEP} mice, we validated IMAGE-predicted TGs for GR in hepatocytes. We further downloaded RNA-seq data from the NCBI-SRA repository (SRP058743) of primary hepatocytes treated 19 h with veh, dex, GW7647 (GW) or a combination of the two ligands (Ratman et al., 2016). We used DESeq2 to determine differentially expressed genes between all conditions (pairwise comparisons, padj < 0.05). We determined if there was a significant interaction between the two ligand treatments for each individual gene using DESeq2 and selected genes that were synergistically induced by the dual dex/GW treatment as genes with a significant interaction that also were significantly induced by the dual treatment compared to vehicle and the single treatments and had a greater log2FC than the sum of the log2FCs induced by the single treatments. Cooperatively induced genes were defined as genes significantly induced by the dual treatment compared to vehicle and single treatments that did not belong to the group of synergistically induced genes.

QUANTIFICATION AND STATISTICAL ANALYSIS

Statistical analyses

Statistical analyses of non-sequencing data were performed using GraphPad Prism software (version 9.2.0). Sequencing data were analyzed in R (3.6.2) with statistical tests as indicated. Further details (including statistical tests and definitions of centers and dispersion) are available in the figure legends. Unless stated otherwise, all bar plots show data as mean ± standard error mean (SEM) and box plots depict the first and third quartiles as the lower and upper bounds of the box, with a thicker band inside the box showing the median value. Whiskers in boxplots indicate either min to max with all data-point shown (< less than 15 data points) or 1.5× the interquartile range (IQR) (> 15 data points), as indicated. Normal distribution of experimental groups at the 0.05 level was evaluated using the D'Agostino-Pearson omnibus normality test and statistically significant outliers was identified using the ROUT method (Q = 5 %). Statistical difference between one comparison of two experimental conditions for normally distributed data was determined using an unpaired t test and a paired t test if the samples were paired. For data not normally distributed, a Wilcoxon rank sum test with continuity correction was applied and a Wilcoxon signed rank test with continuity correction was used to determine if the median of a sample was different from 0. P-values obtained from multiple t test were corrected using the two-stage linear step-up procedure of Benjamini, Krieger and Yekutieli, using an FDR cutoff < 10%. One-way analysis of variance (ANOVA) was used to determine if there were statistically significant differences between three or more independent groups and a 2-way ANOVA was performed to estimate the effect of two different categorical independent variables on one continuous dependent variable. If data were not normally distributed, a Kruskal–Wallis one-way analysis (for unmatched samples) or a Friedman test (for paired samples) were performed. In all cases, the criterion for statistical significance was $p < 0.05$. In post-hoc analyses, p-values were corrected for multiple testing according to Tukey, Dunnett, Dunn or Sidak, as indicated. To investigate the significance of overlap between gene groups, the Fisher's exact test was used for determination of the p values, the odds ratio and the 95% confidence interval. Correlation between two variables was assessed using the Spearman correlation coefficient. No power calculations were used to predetermine sample sizes.